

---

# Long term deformations in soils due to cyclic loading

Andrzej Niemunis<sup>1</sup>, Torsten Wichtmann<sup>1</sup>, and Theodor Triantafyllidis<sup>1</sup>

Institute of Soil Mechanics and Foundation Engineering, Ruhr-University Bochum  
Gebäude IA 4/30, Universitätsstrasse 150, D-44801 Bochum  
Andrzej.Niemunis@rub.de

## 1 Introduction

A substantial accumulation of irreversible strains in soils may appear due to cyclic loading even at relatively small amplitudes. After a large number of cycles the long-term serviceability of structures may be endangered. Under poorly drained conditions, in place of the usual densification, excessive pore pressure is generated. It may lead to soil liquefaction and eventually to a loss of the overall stability. The accumulation effects described by high cycle models refer to a large number ( $> 10^3$ ) of small to moderate total strain amplitudes ( $< 10^{-3}$ ). The phenomenon of accumulation has been described by a high-cycle explicit model. Laboratory testing of high cyclic behaviour is very laborious and therefore most explicit models in the literature are focussed on a very specific practical application only. Compared to them the presented high-cycle model of sand is attempted to be more comprehensive. The performance of the model in calculations of (differential) settlements of shallow foundations is demonstrated.

A cycle (= loop) can be conveniently decomposed into a cumulative part and a resilient part using a hodograph, Fig. 1. We usually speak of strain and stress cycles but the term cycle can be generalized to any state variable (scalar or tensorial)  $\sqcup$ . Having plotted the path  $\sqcup(t)$  we define the *average* value  $\sqcup^{\text{av}}$  to be the centre of the smallest hypersphere that encompasses all  $\sqcup(t)$  within a single period  $T$ . Alternatively,  $\sqcup^{\text{av}}$  can be defined as the middle point between the two most distant states (much easier numerical implementation). The amplitude of a scalar variable is defined as  $\sqcup^{\text{amp1}} = \max|\sqcup - \sqcup^{\text{av}}|$ . A more elegant concept of the *tensorial strain amplitude* is introduced in Section 3. It describes not only the size but also the polarization and the ovality of a cycle.

It turns out that  $\mathbf{D}^{\text{acc}}$  depends strongly on several subtle properties of soil and not on stress and void ratio only. Two new state variables are therefore proposed: the cyclic preloading  $g^A$  which memorizes the amount of fatigue preloading and the back polarization  $\boldsymbol{\pi}$  memorizing the recent orientation of cycles (weighted by their size), see Sections 2.3 and 3.2.

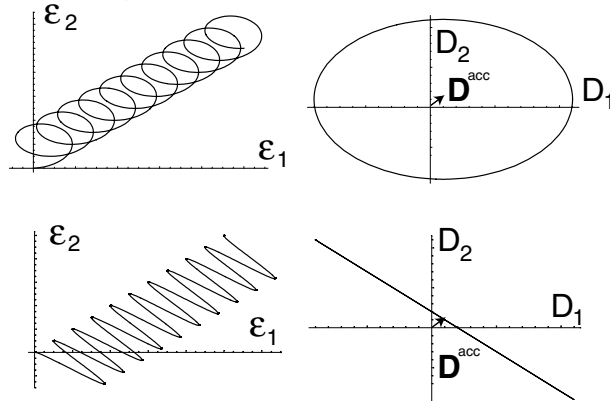


**Fig. 1.** A hodograph is a trajectory of  $\mathbf{D}(t) \approx \dot{\epsilon}$  parametrized with time  $t$ , analogously to the strain path  $\epsilon(t)$ . The rate of accumulation can be easily identified as a drift rate (denoted with arrow) of the average strain upon a cycle. Note that the strain rate is an exactly periodic function  $\mathbf{D}(t) = \mathbf{D}(t + NT)$  whereas the strain  $\epsilon(t)$  is not. The distinction between the cycles encompassing some area ( out-of-phase cycles (= OOP) , above) and the open-curve cycles ( in-phase cycles (= IP), below) will be of importance.

Displacements of structures due to cyclic loading of subsoil are often predicted using *settlement formulas*, e.g. [11, 28]. The settlement  $s(N)$  after  $N$  cycles is extrapolated from the residual settlement  $s_1$  after the first cycle. Various empirical functions, e.g.  $s(N) = s_1 N^C$  or  $s(N) = s_1(1 + C \ln N)$  with a material constant  $C$ , were proposed in the literature. In this paper, we argue that the accumulation depends on numerous factors, see Section 2, which are too complicated to be lumped together into a single parameter  $s_1$ . Moreover, most of the popular settlement formulas are self-contradictory (inconsistent), as demonstrated in Appendix B.

### 1.1 Accumulation as a phenomenon

The phenomenon of *accumulation* manifests itself as a summation of small residual strains ( pseudo-creep) or residual stresses ( pseudo-relaxation). For the two-dimensional case it is shown schematically in Figure 2. If stress cycles are applied, Figure 2a, we observe cyclic pseudo-creep and if strain cycles are applied, Figure 2b, we obtain cyclic pseudo-relaxation. Many laboratory tests are mixed-controlled, so both, pseudo-relaxation and pseudo-creep, may occur simultaneously, Figure 2c. The unspecified term *accumulation* seems, therefore, to be a convenient notion covering the cyclic pseudo-relaxation as well as the cyclic pseudo-creep. In order to understand accumulation in this general sense (independently of the technical aspect how an experiment is

controlled) we have to introduce a constitutive relation (at this place let it be slightly simplified compared to (2))

$$\dot{\mathbf{T}} = \mathbf{E} : (\mathbf{D} - \mathbf{D}^{\text{acc}}), \quad (1)$$

wherein  $\dot{\mathbf{T}}$  is the Zaremba-Jaumann rate of the Cauchy stress,  $\mathbf{D}$  denotes the total stretching,  $\mathbf{E}$  is a pressure-dependent (hypo)elastic stiffness and  $\mathbf{D}^{\text{acc}}$  *would be* the rate of strain accumulation cyclic loading if the experiment were fully stress-controlled. The notation is explained in Appendix A. We have good reasons to express both the intensity of cyclic loading and the accumulation in terms of strain (i.e. of strain amplitude and of strain accumulation rate, respectively). Note, however, that imposing strain (amplitude) we preclude direct observation of strain (accumulation) as a material response. Therefore (1) is indispensable already for the evaluation of laboratory tests, Figure 2. The actually measured response of the material is denoted by superscript  $m$ .

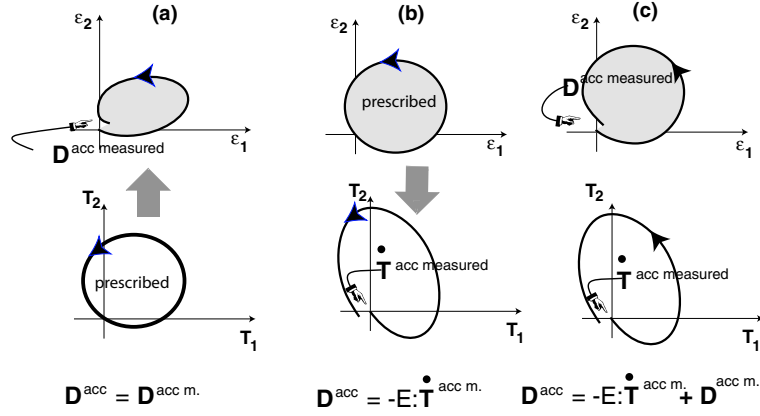


**Fig. 2.**

(a) Stress cycles (= all stress components are prescribed and the stress loop is perfectly closed) leave residual strains.

(b) Strain cycles leave residual stresses.

(c) Mixed control tests leave both residual stresses and residual strains.

Pure accumulation (not superposed by monotonic loading) is considered and therefore  $\mathbf{D}^{\text{pl}}$  can be disregarded. The superscript  $\square^m$  stands for 'measured'.

## 1.2 The high-cycle approach

Two computational strategies are usually followed for dealing with the cyclic loading

- an *implicit calculation* of accumulation

- an *explicit calculation* (or a high-cycle ) of accumulation

The conventional (= implicit) constitutive models describe each loop proceeding by small strain increments. The accumulation of stress or strain appears as a by-product resulting from the fact that the strain or stress loops are not perfectly closed (accumulation is "implied"). Quite sophisticated (e.g. endochronic [39] or multi-surface constitutive models [3, 4, 21]) are usually required. However, their practical applicability is limited by the number of cycles, say  $N = 1000$ , because inevitable cumulative errors ( inaccuracies in the constitutive model and numerical problems resulting from its implementation) become dominant. The high-cycle model proposed in this paper

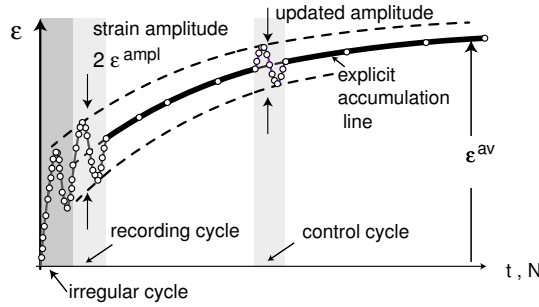


**Fig. 3.** The basic idea of explicit calculation of the cumulative deformation.

follows the other strategy (known also as *N-type* formulation). Explicit models [1, 2, 8, 12, 14, 16–18, 30, 32, 34–37, 40, 44] are similar to the viscoplastic ones in which in place of time  $t$  the number  $N$  of cycles is used. The accumulation of strain due to a package of  $\Delta N$  cycles of a given amplitude is predicted directly. For example, an increment of  $\Delta N = 25$  cycles with the amplitude  $\epsilon^{\text{ampl}} = 10^{-4}$  results in an irreversible strain  $\mathbf{D}^{\text{acc}} \Delta N$  wherein  $\mathbf{D}^{\text{acc}}$  is given by the explicit formula (5). As we shall see, this is the essential equation of the presented model. The explicit strategy is explained in the following flowchart and by Figure 3.

1. Calculate the initial stress field (from self weight and all monotonic loads) in soil. To obtain a realistic initial stress one should use a good model for monotonic loads (not an elastic one).
2. Calculate implicitly two first load cycles (for reasons discussed further in text) recording the strain path  $\epsilon(t)$  in the second one (=first regular cycle) at each integration point. The size of the amplitude is of great importance so one should use a good model for hysteretic behaviour and small-strain nonlinearity (e.g. multi-surface plasticity or, as we do, the extended hypoplasticity [25]).
3. Evaluate the *strain amplitude*. In general case it is a fourth-order tensor  $\mathbf{A}_\epsilon$  discussed in Section 3. The size of the amplitude is assumed constant over

subsequent cycles until it is recalculated in a control cycle. In fresh pluviated samples a clear (up to 15%, [42]) stiffening of soil is observed during the first 100-1000 cycles. Such *conditioning phase* should be considered in the hysteretic model and in this phase the amplitude should be reevaluated more frequently than afterwards.

4. Find the accumulation rate  $\mathbf{D}^{\text{acc}}$  of strain using the explicit formula (5). In the subsequent cycles only the general trend of the accumulation is calculated. This trend is depicted with the thick line in Figure 3.
5. Find the Zaremba-Jaumann stress rate from the constitutive equation

$$\dot{\mathbf{T}} = \mathbf{E} : (\mathbf{D} - \mathbf{D}^{\text{acc}} - \mathbf{D}^{\text{pl}}) \quad (2)$$

and the stress increment  $\Delta\mathbf{T} = \dot{\mathbf{T}}\Delta N$  caused by a package of  $\Delta N$  cycles (= a single increment of the fatigue load). The number of cycles  $N$  is treated as a *continuous* time-like variable so the material "rate" of  $\square$  is understood as its increase "per cycle"

$$\dot{\square} = d\square/dN \quad (3)$$

in the explicit-model context. The Zaremba-Jaumann rate should also be understood "per-cycle". The presence of the conventional plastic strain rate  $\mathbf{D}^{\text{pl}}$  in (2) and the advantage of (2) over (1) is explained in Section 1.3.

The FE program redistributes stress in the course of equilibrium iteration, in effect of which  $\mathbf{D}^{\text{acc}}$  leads to settlements or to pseudo-relaxation, depending on the boundary conditions.

### 1.3 Need for plastic strain rate $\mathbf{D}^{\text{pl}}$

At first it might seem surprising that the plastic stretching  $\mathbf{D}^{\text{pl}}$  caused by monotonic loading and the cumulative stretching  $\mathbf{D}^{\text{acc}}$  are treated separately in (2). Indeed, from the physical point of view they cannot be distinguished. The decomposition of the irreversible strain rate into  $\mathbf{D}^{\text{pl}}$  and  $\mathbf{D}^{\text{acc}}$  is forced by the explicit strategy of calculation. Implicit models need not such separation.

To understand the usefulness of  $\mathbf{D}^{\text{pl}}$  it is instructive to consider a simple 1-dimensional rod made of a tension cut-off material and fixed at both ends. During a cooling process (= thermic shrinkage) tensile stress may occur. However, since no tension is allowed for, the plastic strains are indispensable. In other words, a constitutive model of the form  $\dot{T} = E(D - D^{\text{thermic}} - D^{\text{pl}})$  is required because  $\dot{T} = E(D - D^{\text{thermic}})$  would lead to contradiction with the tension cut-off assumption. At first, one could expect that unlike the thermic deformation, the fatigue loading does not require plastic strains because pseudo-relaxation nudges the stress inward the yield surface. Inferring from element tests, the stress paths could not surpass e.g. the Matsuoka and Nakai [19] yield surface in the process of pseudo-relaxation because the flow rule  $\mathbf{m}$  points to the outside of the yield surface, Figure 7, and therefore the

relaxation  $\dot{\mathbf{T}}^{\text{acc}} = -\mathbf{E} : \mathbf{D}^{\text{acc}}$  tends inwards. However, the absence of  $\mathbf{D}^{\text{pl}}$  does lead to severe problems in FE calculations! Tension or excessive stress ratios may appear if cyclic loading is superposed by a simultaneous monotonic loading which enforces a plastification. Even in boundary value problems under a purely fatigue loading but with a strongly *inhomogeneous spatial distribution* of the accumulation rate (1) can inflict excessive shear or tensile stresses. For example, it is the case if an element that experiences little or no direct fatigue loading itself had a strongly loaded neighbour. The plastic rate  $\mathbf{D}^{\text{pl}}$  would be indispensable in the weakly loaded element to ensure the compliance with the large deformation outside.

The Matsuoka and Nakai [19] yield condition (M-N) with the associated flow rule is used to calculate  $\mathbf{D}^{\text{pl}}$ . First the accumulation rate  $\mathbf{D}^{\text{acc}}$  and the elasto-cumulative predictor

$$\mathbf{T} + \mathbf{E} : (\mathbf{D} - \mathbf{D}^{\text{acc}})\Delta N, \quad (4)$$

should be determined. If a return mapping onto the yield surface is necessary then it must be accompanied by a plastic deformation. The procedure is identical as in elasto-plastic algorithms. The isotropic hypoelastic stiffness  $\mathbf{E}$  with a constant Poisson's ratio ( $\approx 0.2$ ) and with a pressure dependent Young modulus ( $\sim (p/p_{\text{atm}})^{2/3}$ ) is used in (2) and in (4). The *hyperelasticity* is not obligatory in the explicit formulations but it is of great importance, e.g. [24], for implicit models.

#### 1.4 Strain amplitude vs stress amplitude

We have chosen to quantify the magnitude of a cycle in terms of the strain amplitude  $\epsilon^{\text{ampl}}$  rather than of the stress amplitude  $T^{\text{ampl}}$  for three reasons. Firstly,  $T^{\text{ampl}}$  does not provide the sufficient information about large amplitudes. From  $T^{\text{ampl}}$  alone one cannot distinguish between the cycles that are just touching the yield surface and those which penetrate the plastic region, Figure 4. They have the same stress amplitude but very different strain amplitudes and cause different accumulations. Secondly, a usage of  $T^{\text{ampl}}$  would require a reformulation of  $f_p$  (Section 2.5) making it stronger barotropic ( $p$ -dependent). This would be numerically disadvantageous. Thirdly,  $T^{\text{ampl}}$  vanishes at the limit  $\mathbf{T}^{\text{av}} = \mathbf{0}$ , hence the phenomenon presented in Fig. 6 would be omitted.

The amplitude evaluated from the first *irregular cycle* is often untypical. As illustrated in Figure 5a, the strain amplitude obtained from an irregular stress-controlled cycle is too large. Moreover an irregular strain-controlled cycle, Figure 5b, commenced at  $q^{\text{av ini}}$  may strongly affect the average stress,  $q^{\text{av ini}} \rightarrow q^{\text{av}}$ . The subsequent pseudo-relaxation is much slower.

As already mentioned, the high-cycle models are dedicated to problems with a large number of to relatively small amplitudes,  $\epsilon^{\text{ampl}} < 5 \cdot 10^{-3}$ . For

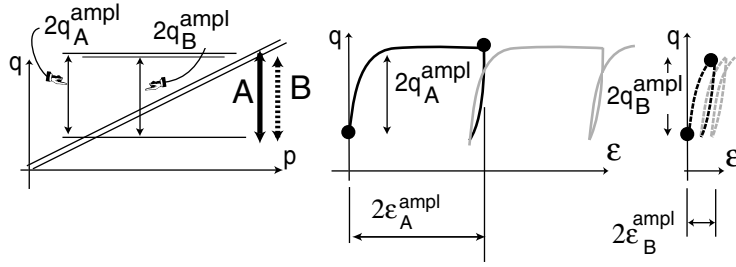


**Fig. 4.** Unsymmetric stress-controlled cycles. The large cycles A (solid line) which encounter the yield surface (double line) are poorly described by the stress amplitude  $q_A^{\text{ampl}}$  alone. The stress path B (dotted line) which approaches only the yield surface without touching it has almost the same stress amplitude  $q_B^{\text{ampl}} \approx q_A^{\text{ampl}}$  but the respective strain amplitudes are quite different and so are the rates of accumulation.

large amplitudes alternating plasticity may occur and the rate of strain accumulation  $\mathbf{D}^{\text{acc}}$  (including direction  $\mathbf{m}$ ) depends essentially on the asymmetry of the strain loop. In such case the description given by (6) and (7) becomes inaccurate. Similarly, for stresses in the vicinity of the yield surface, even relatively small strain cycles may cause the progressive failure which is an accumulation much faster than the one described by (7). For these reasons the FE routine should control whether the yield surface is encountered during the implicit calculation (item 2 in the flowchart in Section 1.2) or not. If so, (7) is not applicable and the residual strain  $\mathbf{D}^{\text{acc}}$  should be found from *direct extrapolation*. This means that the estimation (5) is replaced by  $\mathbf{D}^{\text{acc}} = \mathbf{D}^{\text{acc m}} - \mathbf{E} : \overset{\circ}{\mathbf{T}}^{\text{acc m}}$ , wherein the recorded residuals are denoted with superscript  $\square^{\text{m}}$ , cf. Figure 2c.

## 2 Explicit formula for $\mathbf{D}^{\text{acc}}$

The essential element of the presented model is the explicit formula (5). Before presenting details of this semi-empirical equation let us consider the advantage of expressing the general notion of accumulation with  $\mathbf{D}^{\text{acc}}$  and not with the stress rate  $\overset{\circ}{\mathbf{T}}$ , let alone with the accumulated pore pressure. Our argument is based on an experiment, Figure 6, showing that  $\mathbf{D}^{\text{acc}}$  need *not* vanish with the effective stress, i.e. for  $\mathbf{T} = \mathbf{0}$ . The pore pressure build-up would be even a worse choice because it describes merely the isotropic pseudo-relaxation.

Our experiments [27, 38, 41–43] show that  $\mathbf{D}^{\text{acc}}$  depends on a number of factors which can be treated independently and which can be combined into the following multiplicative form

$$\mathbf{D}^{\text{acc}} = \mathbf{m} f_{\text{ampl}} \dot{f}_N f_p f_Y f_e f_\pi. \quad (5)$$

The scalar functions  $f_{\text{ampl}}$ ,  $\dot{f}_N$ ,  $f_p$ ,  $f_Y$ ,  $f_e$  and  $f_\pi$  describe the influence of the strain amplitude  $\epsilon^{\text{ampl}}$ , the number of cycles  $N$ , the average mean pressure

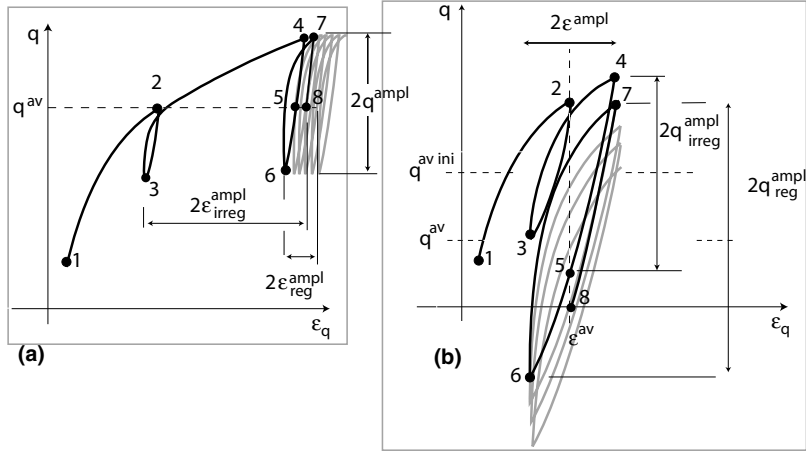


**Fig. 5.** (a) Unsymmetric stress-controlled cycles. (b) Unsymmetric strain-controlled cycles. Monotonic loading 1-2 is followed by the irregular cycle (2-3-4-5) and the regular cycle (5-6-7-8). In the irregular stress-controlled cycle the strain amplitude  $\epsilon_{irreg}^{ampl}$  is too large. In the irregular strain-controlled cycle the stress amplitude is too small and, which is more important, the average stress changes from  $q^{av\ ini}$  to  $q^{av}$ .

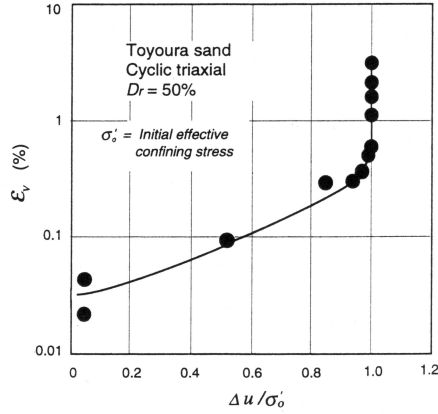


**Fig. 6.** Experimental evidence that the accumulation of strain continues also at vanishing effective stress  $\mathbf{T} = \mathbf{0}$ , see Shamoto [33]. During cyclic loading under undrained conditions the excess pore pressure  $\Delta u$  increases up to the initial effective stress  $\sigma_0$ . Then all components of the effective stress must vanish (the soil is liquefied). The additional increase of volumetric strain from  $\epsilon_v = 0.5\%$  to  $\epsilon_v = 4\%$ , measured during the subsequent isotropic reconsolidation, indicates that the soil skeleton must undergo a latent densification in the liquefied stage, i.e. for  $\mathbf{T} = \mathbf{0}$ .

$p^{\text{av}}$ , the average stress ratio, the void ratio  $e$ , and the change of the polarization of the strain loop, respectively. The unit tensor  $\mathbf{m}$  expresses the flow rule. The validity of the above empirical formula has been checked within the range of all performed tests. The amplitudes were varied within the range  $5 \cdot 10^{-5} < \epsilon^{\text{ampl}} < 5 \cdot 10^{-3}$  and the average stresses between  $50 \leq p^{\text{av}} \leq 300$  kPa for triaxial compression as well as for triaxial extension. In the following subsections the components of (5) are discussed.

## 2.1 Direction of accumulation $\mathbf{m}$

The accumulation  $\mathbf{D}^{\text{acc}}$  has a volumetric portion but also a significant deviatoric component [35, 42]. Since the ratio between the deviatoric and the volumetric accumulation has been observed to be almost constant for a given stress  $\mathbf{T}^{\text{av}}$ , Figure 7, it seems reasonable to define a kind of flow rule  $\mathbf{m}(\mathbf{T}^{\text{av}}) = \mathbf{D}^{\text{acc}}$ . The unit tensor  $\mathbf{m}$  points in the direction of accumulation in the strain space. The coaxiality between  $\mathbf{D}^{\text{acc}}$  and  $\mathbf{T}$  is analogous to the coaxiality of  $\mathbf{D}^{\text{pl}}$  and  $\mathbf{T}^{\text{av}}$  in the plasticity theory. The direction  $\mathbf{m}$  has been found independent of the void ratio  $e$ , of the amplitude  $\epsilon^{\text{ampl}}$  and of the polarization  $\mathbf{A}_\epsilon$  etc. The flow rule may slightly vary with increasing number of cycles  $N$ , Figure 7, but this fact has been disregarded in the present version of the model. Judging by the triaxial tests presented in Figure 7, the direction of accumulation  $\mathbf{m}$  is well approximated by the associated flow rule

$$\mathbf{m} \sim -\frac{1}{3}\left(p - \frac{q^2}{M^2 p}\right) \mathbf{1} + \frac{3}{M^2} \mathbf{T}^* \quad (6)$$

from the modified Cam-clay model [31] with the Roscoe's invariants  $p, q$  and the critical state line inclined at  $M = \frac{6 \sin \varphi_c}{3 \pm \sin \varphi_c}$ . The experiments [42] show that the accumulation is dilative beyond the critical state line,  $|q/p| > M$ , which is in accordance with (6).

## 2.2 Influence factor $f_{\text{ampl}}$ of the amplitude

The rate of accumulation depends essentially on the amplitude which enters (5) via  $f_{\text{ampl}}$ . The factor  $f_{\text{ampl}}$  describes the influence of the *size*  $\epsilon^{\text{ampl}}$  of the amplitude (= scalar value). For IP-cycles  $\epsilon^{\text{ampl}} = \|\epsilon^{\text{ampl}}\|$  and for OOP-cycles  $\epsilon^{\text{ampl}} = \|\mathbf{A}_\epsilon\|$ , see Section 3. Figure 8 shows that the accumulation rate is proportional to the square of the strain amplitude. This proportionality is valid up to  $\epsilon^{\text{ampl}} = 10^{-3}$ . A few tests with very large amplitudes show that the accumulation rate remains almost constant above this limit. Therefore we propose

$$f_{\text{ampl}} = \begin{cases} \left(\frac{\epsilon^{\text{ampl}}}{\epsilon_{\text{ref}}^{\text{ampl}}}\right)^2 & \text{for } \epsilon^{\text{ampl}} \leq 10^{-3} \\ 100 & \text{otherwise,} \end{cases} \quad (7)$$

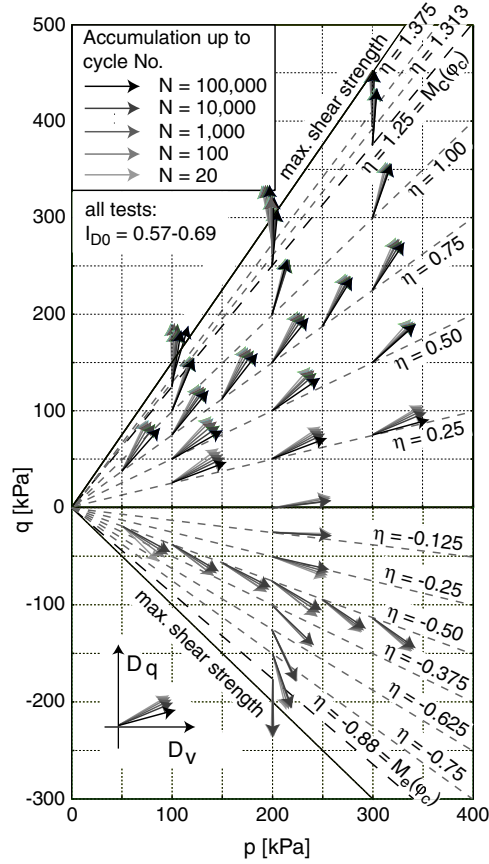


**Fig. 7.** Directions  $\mathbf{m}$  of strain accumulation were determined from numerous cyclic triaxial tests for various stress ratios  $\eta^{\text{av}} = q^{\text{av}}/p^{\text{av}}$ . The initial index of density of a sample is denoted by  $I_{D0}$ .

wherein the reference amplitude is  $\epsilon_{\text{ref}}^{\text{ampl}} = 10^{-4}$ . Equation (7) has been found valid for the range  $5 \cdot 10^{-5} < \epsilon^{\text{ampl}} < 5 \cdot 10^{-3}$ .

According to some literature [15,32,41] the volumetric portion  $\epsilon_P^{\text{ampl}}$  of the amplitude has less influence on the rate of accumulation than the deviatoric one  $\epsilon_Q^{\text{ampl}}$  (see Appendix A for definition of isomorphic components). However, reinterpretation of our earlier tests with the careful consideration of the membrane penetration effect [22] has revealed that  $\epsilon_P^{\text{ampl}}$  and  $\epsilon_Q^{\text{ampl}}$  contribute equally(!) to the accumulation and need not be treated separately. Hence,

$$\epsilon^{\text{ampl}} = \sqrt{(\epsilon_Q^{\text{ampl}})^2 + (\epsilon_P^{\text{ampl}})^2} \text{ can be directly substituted into (7).}$$

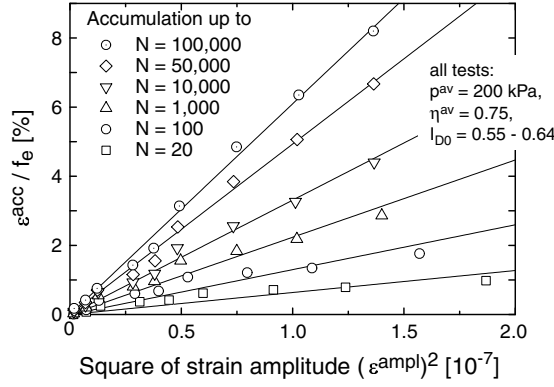


Fig. 8. The rate of accumulation is proportional to the square of the strain amplitude. The diagram has been purified from the variability of  $f_e$ .

### 2.3 Cyclic history factor $f_N$

The rate of accumulation depends strongly on the *cyclic preloading*, i.e. on the number of cycles applied in the past, on their polarization and the size. Figure

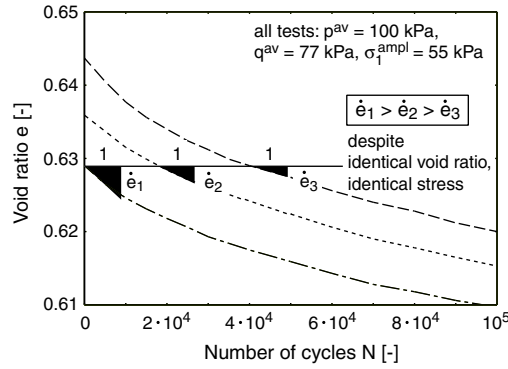


Fig. 9. The effect of cyclic loading history on the rate of densification  $\dot{e} = de/dN$  measured during cyclic drained triaxial test.

9 shows the compaction curves of three triaxial samples which have different densification rates  $\dot{e}$  (rates of change of the void ratio  $e$ ) passing through the same void ratio  $e = 0.629$ . The average stress and the amplitude are identical so that the only reason for the observed difference can be the cyclic preloading which renders the accumulation slower.

In order to consider the cyclic preloading two additional state variables have been introduced: the scalar  $g^A$  for the number of cycles  $N$  and their size  $\epsilon^{ampl}$  and the tensor  $\pi$  for the recent polarization. Both state variables are

phenomenological, i.e. we do not investigate whether they are related to the number of grain contacts and their directional distribution, the spatial fluctuation of stress, internal systems of shear bands etc. The major disadvantage of non-physical state variables is that they cannot be directly measured. They must be estimated by their effects. In particular, the initial *in-situ* value of  $g^A$  can be correlated [38] to the liquefaction potential [13]. The discussion of  $\pi$  is deferred until Section 3 and we continue with the scalar state variable  $g^A$  here.

In tests on freshly pluviated samples, the cyclic history (number and size of all applied cycles) is known and one can determine exactly how the number of cycles slows down the accumulation rate. For strain cycles of constant amplitude, the increase of the total strain accumulated after  $N$  cycles, see

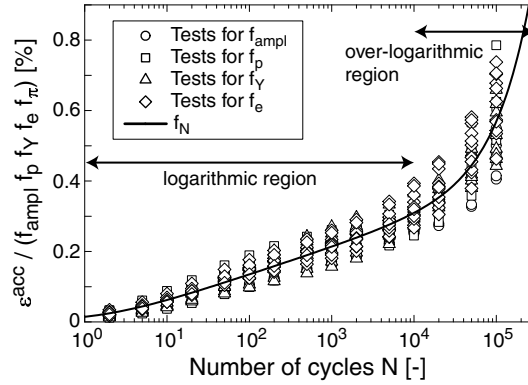


**Fig. 10.** Accumulated strain  $\varepsilon^{\text{acc}}$  divided by the functions  $f_{\text{ampl}}$ ,  $f_p$ ,  $f_Y$ ,  $f_e$  and  $f_\pi$  as a function of the number of cycles.

Figure 10, can be well approximated by the empirical formula

$$f_N = C_{N1} [\ln(1 + C_{N2}N) + C_{N3}N] \quad \text{or in rates:} \quad (8)$$

$$\dot{f}_N = C_{N1} \left[ \frac{C_{N2}}{1 + C_{N2}N} + C_{N3} \right] \quad (9)$$

with three material constants  $C_{N1}$ ,  $C_{N2}$  and  $C_{N3}$  (the latter is important for a large number of cycles only). Equation (8) is an already purified curve without the concurrent effects due to changes in the void ratio, stress, etc.

#### 2.4 Miner's rule and the state variable $g^A$

Although the rate of accumulation depends strongly on the number  $N$  of cycles in the past it is not a good idea to treat  $N$  as a new state variable. Doing so the product of  $f_{\text{ampl}}$  and  $\dot{f}_N$  given by (7) and (9) would severely contradict the Miner's rule [20].

Originally the Miner's rule pertains to the fatigue of metals and generalizes the Wöhler's curve. The Wöhler's SN-curve shows the number  $N_f$  of uniaxial cycles with a stress amplitude  $S = T_1^{\text{ampl}} = \text{const}$  that causes failure. The Palmgren-Miner's rule describes an analogous condition for several blocks of cycles with constant amplitudes within each block. Suppose we have  $n$  blocks of cycles. In the  $i$ -th block the number of actually applied cycles is  $N_i$  and their amplitude  $A_i$  is constant. Suppose also that we know the numbers  $N_{fi}$  of cycles to failure for each amplitude  $A_i$ . The Miner's rule excludes failure if inequality

$$\sum_{i=1}^n \frac{N_i}{N_{fi}} < 1 \quad (10)$$

is satisfied. The Miner's rule implies that:

- the sequence of application of constant-amplitude blocks is of no importance,
- the periodic strain loop can be decomposed into several *convex* loops (e.g., using the so-called rainflow algorithm). These convex loops can be applied sequentially as separate blocks with constant amplitudes.

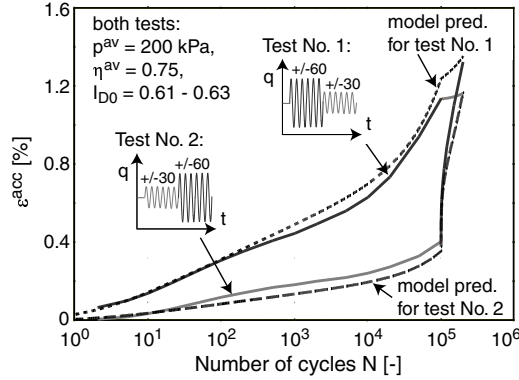


**Fig. 11.** Numerical calculation and experimental verification of the Miner's rule.

It is controversial whether sands obey the Miner's rule very rigorously. However, in one case the inconsistency between (9) and the Miner's rule is unacceptable, namely for a combination of a package of  $N_1$  cycles with  $\epsilon_{(1)}^{\text{ampl}}$  and a package of  $N_2$  cycles with almost vanishing amplitude  $\epsilon_{(2)}^{\text{ampl}} \approx 0$ . The total accumulation should be independent of the sequence of application of these packages because it does not matter whether we *do nothing* after or before the actual loading with  $\epsilon_{(1)}^{\text{ampl}} > 0$ . The vanishingly small cycles should have

no effect at all. However, (9) unwisely disregards the sizes of amplitudes *in the past*.

A state variable memorizing the number of cycles together with their amplitudes is therefore required. Though a simple concept [32] of using the product  $(\epsilon^{\text{ampl}})^2 N$  instead of  $N$  in (9) obeys the Miner's rule, it is in conflict with (7), cf. [27]. The variable  $g^A$ , proposed in the following, is a compromise solution. We consider the product of  $f_{\text{ampl}}$  and  $\dot{f}_N$  denoting it as  $\dot{g} = f_{\text{ampl}} \dot{f}_N$ . Functions  $f_{\text{ampl}}$  and  $\dot{f}_N$  are further on given by (7) and (9). Note that only a part of  $\dot{g}$  depends on  $N$  namely  $\dot{g}^A = f_{\text{ampl}} C_{N1} C_{N2} / (1 + C_{N2} N)$ . Integrating  $\dot{g}$  with respect to  $N$  one obtains

$$g = \overbrace{f_{\text{ampl}} C_{N1} \ln(1 + C_{N2} N)}^{=g^A} + \overbrace{f_{\text{ampl}} C_{N1} C_{N3} N}^{=g^B} \quad (11)$$

The idea is to reformulate (9) replacing  $N$  by  $g^A$ . For this purpose we solve  $g^A = g^A(N)$  for  $N$  and substitute the result into the expression for  $\dot{g}$ , viz.

$$\dot{g} = f_{\text{ampl}} C_{N1} C_{N2} \exp\left(-\frac{g^A}{C_{N1} f_{\text{ampl}}}\right) + f_{\text{ampl}} C_{N1} C_{N3}, \quad (12)$$

wherein  $f_{\text{ampl}}$  refers to the current amplitude and  $g^A$  contains the information about the amplitudes in the past and the respective numbers of cycles. By this expedient the Miner's rule is satisfied at the limit of very small amplitudes and (9) remains valid for the special case of  $\epsilon^{\text{ampl}} = \text{const}$ .

A numerical simulation of the accumulation caused by two blocks of cycles with different amplitudes and applied in different sequences gives almost the same total accumulation, so it is in agreement with the Miner's rule and with the experiment, see Figure 11.

Presumably apart from the cyclic preloading the static preloading [6] is also of importance and should be investigated in future.

## 2.5 Empirical factors $f_p$ and $f_Y$ for stress and factor $f_e$ for void ratio

The rate of accumulation depends on the average stress ratio  $\hat{\mathbf{T}}^{\text{av}} = \mathbf{T}^{\text{av}} / \text{tr}(\mathbf{T}^{\text{av}})$ , on the average mean stress  $p^{\text{av}}$  and the void ratio  $e$ . It turns out that one can treat these effects separately and use the product  $f_Y f_p f_e$  of the respective functions. As it might be expected, the rate of accumulation increases with the stress obliquity  $\mathbf{T} / \text{tr} \mathbf{T}$ , especially if the yield surface is approached. This dependence, Figure 12, can be approximated by

$$f_Y = \exp(C_Y \bar{Y}^{\text{av}}) \quad \text{with} \quad C_Y \approx 2 \quad (13)$$

wherein

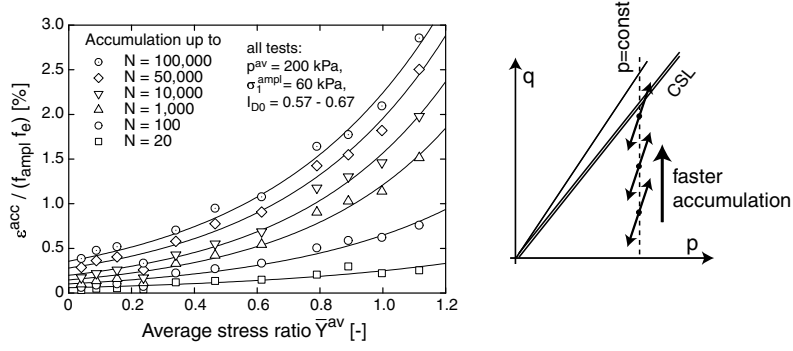


**Fig. 12.** Accumulated strain  $\varepsilon^{\text{acc}}$  as a function of the average stress ratio  $\bar{Y}^{\text{av}}$  for different numbers of cycles. These purified diagrams do not contain the variability due to  $f_{\text{ampl}}$  and  $f_e$ .

$$\bar{Y} = \frac{Y - 9}{Y_c - 9}, \quad Y = -\frac{I_1 I_2}{I_3} \quad \text{and} \quad Y_c = \frac{9 - \sin^2 \varphi_c}{1 - \sin^2 \varphi_c}. \quad (14)$$

is based on the function by Matsuoka and Nakai. The stress invariants  $I_1, I_2, I_3$  are functions of  $\mathbf{T}^{\text{av}}$  defined in Appendix A and the critical friction angle is denoted by  $\varphi_c$ .

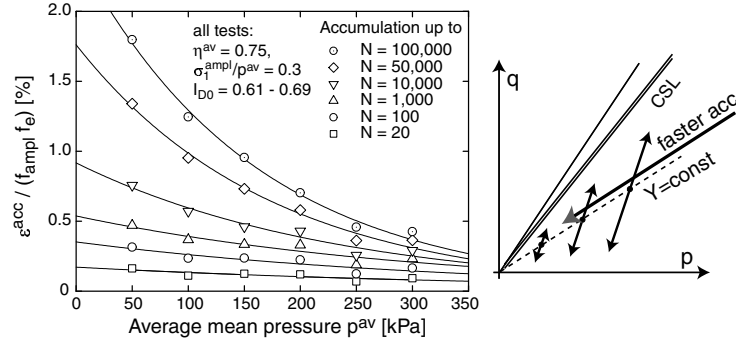


**Fig. 13.** Accumulated strain  $\varepsilon^{\text{acc}}$  in dependence on the average mean pressure  $p^{\text{av}}$  for different numbers of cycles. The diagrams have been purified from the variability of  $f_{\text{ampl}}$  and  $f_e$ .

The accumulation rate becomes smaller(!) with  $p^{\text{av}}$ . The experimental results, Figure 13, can be approximated by

$$f_p = \exp \left[ -C_p \left( \frac{p^{\text{av}}}{p_{\text{atm}}} - 1 \right) \right] \quad (15)$$

wherein  $p_{\text{atm}} = 100$  kPa and the material constant is  $C_p \approx 0.43$ . The validity of (13) and (15) has been tested for  $50 \leq p^{\text{av}} \leq 300$  kPa. Of course, loose sands

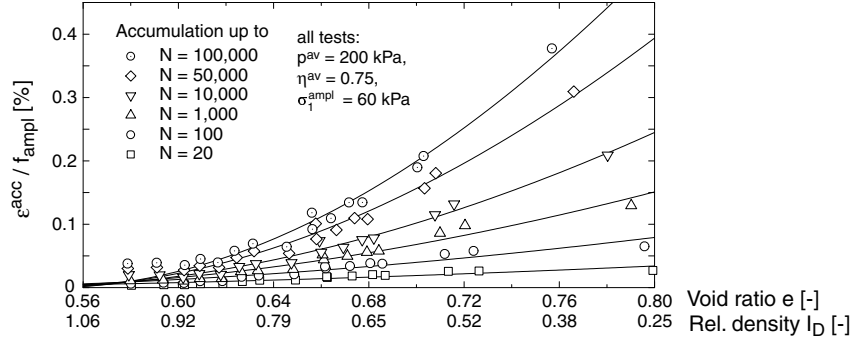


**Fig. 14.** Accumulated strain  $\varepsilon^{\text{acc}}$  in dependence on the void ratio  $e$  for different numbers of cycles. The  $f_{\text{amp1}}$ -variability has been removed here.

can be easier compacted than dense ones. This is confirmed by experimental results, Figure 14, which can be approximated by

$$f_e = \frac{(C_e - e)^2}{1 + e} \frac{1 + e_{\text{ref}}}{(C_e - e_{\text{ref}})^2} \quad (16)$$

with the material constants  $e_{\text{ref}} = 0.874$  and  $C_e = 0.54$ . The factors  $f_p$  and

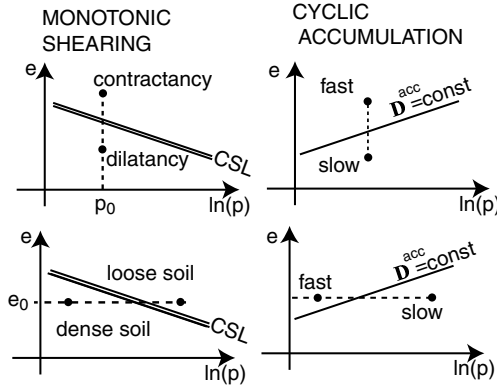


**Fig. 15.** Lines of constant rate of accumulation in the  $e - \ln p$  diagram are differently inclined than the CSL. The notions loose sand and dense sand are pressure-dependent in the critical state soil mechanics. For cyclic accumulation this dependence is not analogous.

$f_e$  cannot [27] be described using the 'distance to the critical state line' in the  $e - \ln p$  diagram. For a given void ratio  $e$ , sand contracts faster under monotonic shearing when  $p$  is larger. Under cyclic loading it is vice versa, see Figure 15.

## 2.6 Sensitivity of $D^{\text{acc}}$

In the previous sections we have presented various factors that influence the rate of accumulation. They have been examined in the laboratory and, one by one, approximated by simple formulas. A legitimate question is whether all these factors are really necessary in the model, because the determination of the material constants requires a considerable effort<sup>1</sup>. Table 1 summarizes the presented results showing the expected variability of the functions  $f_{\text{ampl}}$ ,  $f_N$ ,  $f_p$ ,  $f_Y$ ,  $f_e$  and  $f_\pi$  for the typical range of input parameters.

**Table 1.** Summary of the factors  $f_i$  and a list of the material constants  $C_i$  for the tested sand.

Function	Mat. constants	typical range of response	remarks
$f_{\text{ampl}} = \left( \frac{\epsilon^{\text{ampl}}}{\epsilon_{\text{ref}}^{\text{ampl}}} \right)^2$ or (7)	$\epsilon_{\text{ref}}^{\text{ampl}}$	$10^{-4}$	$0 \dots 100$
$f_N = \frac{C_{N1}C_{N2}}{1 + C_{N2}N} + C_{N1}C_{N3}$	$C_{N1}$ $C_{N2}$ $C_{N3}$	$3.4 \cdot 10^{-4}$ $0.55$ $6.0 \cdot 10^{-5}$	$(0.1 \dots 0.2) 10^{-3}$ $0 < N < \infty$
$f_p = \exp -C_p \frac{p^{\text{av}}}{p_{\text{atm}}} - 1$	$C_p$ $p_{\text{atm}}$	$0.43$ $100 \text{ kPa}$	$1.5 \dots 0.02$ $50 \leq p \leq 300 \text{ kPa}$
$f_Y = \exp C_Y Y^{\text{av}}$	$C_Y$	$2.0$	$1 \dots 7.4$ $0 < Y < 1.1$
$f_e = \frac{(C_e - e)^2}{1 + e} \frac{1 + e_{\text{ref}}}{(C_e - e_{\text{ref}})^2}$	$C_e$ $e_{\text{ref}}$	$0.54$ $0.874$	$1 \dots 0$
$f_\pi = 1 + C_{\pi 1} \left[ 1 - \frac{\vec{\mathbf{A}}_\epsilon :: \boldsymbol{\pi}}{\boldsymbol{\pi} + \Delta \boldsymbol{\pi} = \mathcal{R} : \boldsymbol{\pi}} \right]$ $\boldsymbol{\pi} + \Delta \boldsymbol{\pi} = \mathcal{R} : \boldsymbol{\pi}$ with (24)	$C_{\pi 1}$ $C_{\pi 2}$	$4.0$ $200$	$1 \dots 4$ quickly declines

Evidently, all presented factors may strongly influence the rate of accumulation and therefore their incorporation into the model seems justified.

## 3 Out-of-phase cycles and polarization

We distinguish between *in-phase* (= IP) strain cycles and *out-of-phase* (= OOP) cycles. The IP-cycles can be defined by the equation

$$\boldsymbol{\epsilon} = \boldsymbol{\epsilon}^{\text{av}} + \boldsymbol{\epsilon}^{\text{ampl}} f(t), \quad (17)$$

<sup>1</sup> In the continuation of this work we intend to facilitate the determination of the material constants giving correlations to the angularity, asperity and to the grain size distribution.

wherein  $\epsilon^{\text{ampl}}$  contains the amplitudes of the individual components, i.e.  $(\epsilon^{\text{ampl}})_{ij} = (\epsilon_{ij})^{\text{ampl}}$ . All components of  $\epsilon$  given by (17) oscillate together according to the same scalar periodic function, e.g.  $f(t) = \sin(t)$  which is varying between -1 and 1. IP-cycles that have only one non-zero eigenvalue of  $\epsilon^{\text{ampl}}$  are termed *uniaxial*, otherwise they are *multiaxial*.

The out-of-phase (=OOP) cycles cannot be expressed by (17), e.g.

$$\epsilon(t) = \epsilon^{\text{av}} + \begin{pmatrix} \epsilon_{11}^{\text{ampl}} \sin(t) & 0 & 0 \\ 0 & \epsilon_{22}^{\text{ampl}} \sin(t + \theta) & 0 \\ 0 & 0 & 0 \end{pmatrix}. \quad (18)$$

Due to the phase shift  $\theta \neq n\pi$ , the OOP strain loop (18) encloses some area in the strain space (the shadowed area(s) in Figure 2). The shape of a strain cycle is of importance for the accumulation (similar effect is known in the fatigue analysis of metals [7, 29]).

The rate of accumulation depends on the orientation of the strain loop (= polarization) and its ovality (= shape). It is also important how many dimensions of the strain space are penetrated by the OOP strain cycle.

Practical cases involving OOP cycles are not rare, e.g. Rayleigh waves, moving vehicles, etc. Even during conventional cyclic triaxial tests with a constant cell pressure OOP cycles may (unintentionally) occur due to the variable dilatancy. Unfortunately, OOP cycles cannot be performed easily in the laboratory and they are rarely addressed to in the literature [5, 41].

Our goal is to incorporate the information about the shape and the polarization of the strain loop into the novel *tensorial definition* of the strain amplitude  $A_\epsilon$ . It is based on tests performed in the triaxial cell with periodic changes of both, lateral and axial stress. Moreover, several special tests have been done using an extended direct simple shear (DSS) device [41].

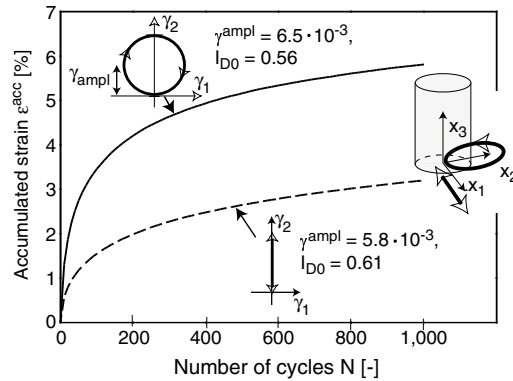


**Fig. 16.** Circular strain loops generate approximately twice faster accumulation than the in-phase ones.

### 3.1 Tensorial amplitude $\mathbf{A}_\epsilon$

The OOP cycles produce more accumulation than the IP cycles of the same size, e.g. the accumulation caused by the loop (18) with the phase shift  $\theta = 90^\circ$  is larger than the accumulation due to an IP loop of the size  $\max(\epsilon_{11}^{\text{ampl}}, \epsilon_{22}^{\text{ampl}})$ , see Figure 16. According to several DSS and triaxial tests [41], the accumulation caused by two-dimensional harmonic OOP cycles is equivalent to the total effect of the orthogonal IP cycles into which the strain loop could be decomposed. In particular, the accumulation caused by two-dimensional cycles (18) could be estimated using  $f_{\text{ampl}} \sim (\epsilon_{11}^{\text{ampl}})^2 + (\epsilon_{22}^{\text{ampl}})^2$ . Analogously, for an OOP cycle

$$\epsilon(t) = \epsilon^{\text{av}} + \begin{pmatrix} \epsilon_{11}^{\text{ampl}} f_{11}(t) & \epsilon_{12}^{\text{ampl}} f_{12}(t) & \epsilon_{13}^{\text{ampl}} f_{13}(t) \\ \epsilon_{21}^{\text{ampl}} f_{21}(t) & \epsilon_{22}^{\text{ampl}} f_{22}(t) & \epsilon_{23}^{\text{ampl}} f_{23}(t) \\ \epsilon_{31}^{\text{ampl}} f_{31}(t) & \epsilon_{32}^{\text{ampl}} f_{32}(t) & \epsilon_{33}^{\text{ampl}} f_{33}(t) \end{pmatrix} \quad (19)$$

with six harmonic functions  $f_{ij}(t) = \sin(\omega t + \theta_{ij})$ , i.e. with a common period  $2\pi/\omega$  but with various phase shifts  $\theta_{ij}$ , the size of the amplitude can be evaluated from the norm of the matrix composed of the amplitudes, i.e.

$$\epsilon^{\text{ampl}} = \sqrt{\epsilon_{ij}^{\text{ampl}} \epsilon_{ij}^{\text{ampl}}} \quad (20)$$

Note that  $\epsilon_{ij}^{\text{ampl}}$  denotes the amplitude of the  $ij$ -th component of strain,  $\epsilon_{ij}^{\text{ampl}} = \max|\epsilon_{ij}(t) - \epsilon_{ij}^{\text{av}}|$  and not the  $ij$ -th component of a "tensorial amplitude".

Now, a generalization of (20) for arbitrary periodic functions  $f_{ij}$  is proposed, i.e. the oscillations need not be harmonic. Moreover, if the accumulation is investigated using the FE method then the analytical form (19) is not known. Suppose, we are given a strain loop in form of a sequence of discrete strains  $\epsilon(t_k)$ ,  $k = 1, \dots, M$  recorded by an FE program at a Gauss point. In order to formulate a suitable definition of the tensorial amplitude  $\mathbf{A}_\epsilon$  we keep in mind the following observations:

- The shape of the strain cycle, Figure 16, influences the accumulation rate.
- The orientation (= polarization) of the cycle in the strain space is of importance, Figure 17. A sudden change of the polarization may increase the rate of accumulation [41].
- The strain states upon a cycle need not be coaxial and therefore the paths  $\epsilon(t)$  are 6-dimensional.
- The size of the 6-dimensional strain path must be described by 6 extents (further called *spans*).
- Polarization cannot have a sign, i.e. it has a direction but no *sense of the direction*.

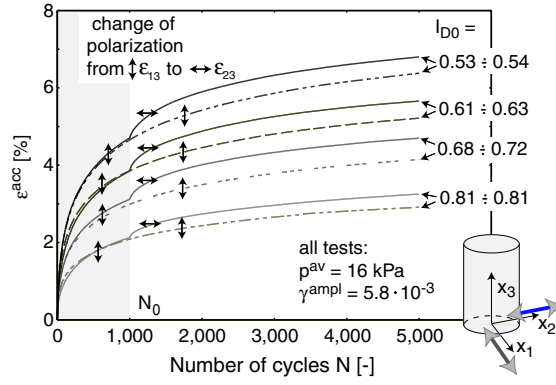


Fig. 17. After a sudden change of polarization  $\mathbf{A}_\epsilon$  the rate of accumulation leaps.

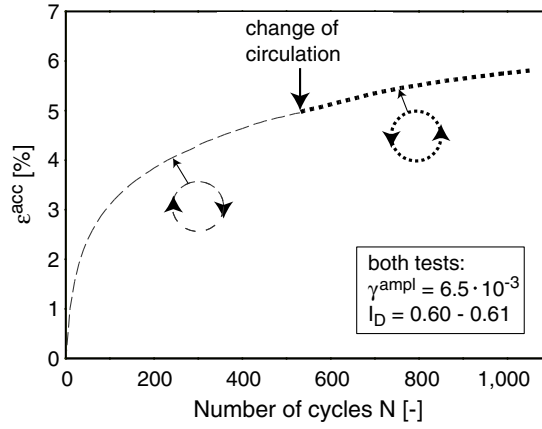


Fig. 18. A change of the circulation of the cyclic strain path does not affect the accumulation.

- A change of circulation has no effect. Figure 18 does not show any change of the accumulation rate after the circulation was changed from the clockwise  $\odot$  to the counterclockwise  $\ominus$ ,

From a recorded cycle  $\epsilon(t_k)$  with  $k = 1, \dots, M$  we may determine the pair of the two most distant points, say  $\epsilon(t_a)$  and  $\epsilon(t_b)$ . The span of the cycle is quantified by its size  $2R^{(6)} = \|\epsilon(t_a) - \epsilon(t_b)\|$  and its orientation  $\mathbf{r}^{(6)} = (\epsilon(t_a) - \epsilon(t_b))$ . The upper index  $\sqcup^{(i)}$  corresponds to the maximum possible number of dimensions of the loop, e.g. the original strain path (before flattening) can be at most six-dimensional,  $\epsilon^{(6)} = \epsilon$ . In order to find the second longest span the strain loop is *projected* onto the hyperplane perpendicular to  $\mathbf{r}^{(6)}$ . It results in the flattened strain trajectory  $\epsilon^{(5)} = \epsilon^{(6)} - \mathbf{r}^{(6)} : \epsilon^{(6)} \otimes \mathbf{r}^{(6)}$  which has at most five dimensions. The span of the flattened trajectory can be determined analogously and described by  $R^{(5)}$  and  $\mathbf{r}^{(5)}$ . The flattened loop

is subjected to the subsequent projection, this time along  $\mathbf{r}^{(5)}$ , etc. Of course  $R^{(6)} \geq R^{(5)} \geq \dots \geq R^{(1)}$  holds.

The tensorial amplitude  $\mathbf{A}_\epsilon$  is proposed to be defined as the following sum

$$\mathbf{A}_\epsilon = \sum_{i=1}^6 R^{(i)} \mathbf{r}^{(i)} \otimes \mathbf{r}^{(i)}. \quad (21)$$

collecting all spans<sup>2</sup>. Briefly speaking, the described method consists in a

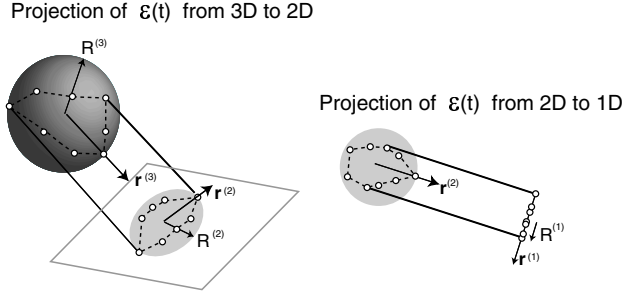


Fig. 19. The directions  $\mathbf{r}_i$  and the sizes  $R^{(i)}$  of the strain loop.

gradual degeneration of the strain path in order to determine its spans. The sense of the direction of  $\mathbf{r}^{(i)}$  is of no importance, which is obvious from (21). For numerical efficiency the calculation can be aborted if the size of the subsequent span is negligible (say less than 10% of the largest span). Projections from a 3-dimensional path to the 1-dimensional path are shown in Figure 19.

From the above algorithm a list of radii  $R^{(6)} \geq R^{(5)} \geq \dots \geq R^{(1)}$  and a list of mutually orthogonal orientations:

$\mathbf{r}^{(6)}, \mathbf{r}^{(5)}, \dots, \mathbf{r}^{(1)}$  are obtained. Substituted into (21) they constitute the tensorial amplitude. The amplitude  $\mathbf{A}_\epsilon$  is a 4-th order tensor which has the eigenvalues  $R^{(i)}$  and the corresponding eigentensors  $\mathbf{r}^{(i)}$ .

The normalized amplitude

$$\mathbf{A}_\epsilon = \mathbf{A}_\epsilon / \|\mathbf{A}_\epsilon\| \quad (22)$$

is called *polarization* and the norm

$$\epsilon^{\text{amp1}} = \|\mathbf{A}_\epsilon\| = \sqrt{(R^{(6)})^2 + (R^{(5)})^2 + \dots + (R^{(1)})^2} \quad (23)$$

is the scalar amplitude. For harmonic cycles of type (19), definition (23) simplifies to (20). This has been demonstrated in [26].

<sup>2</sup> An analogous definition using the  $\frac{1}{4}$ -th of the perimeters  $P^{(i)}$  of the loops instead of the radii  $R^{(i)}$  lead to a worse approximation of the experiments.

### 3.2 Back polarization $\pi$ and function $f_\pi$

If a package of cycles with the amplitude  $\mathbf{A}_\epsilon^{(1)}$  is directly followed by another package with the amplitude  $\mathbf{A}_\epsilon^{(2)}$  with the same polarization, i.e.  $\mathbf{A}_\epsilon^{(1)} :: \mathbf{A}_\epsilon^{(2)} = 1$ , no correction of the accumulation rate is needed ( $f_\pi = 1$ ) except for  $f_{\text{ampl}}$ . However, if the polarization has changed then the above product may become significantly smaller (in the extreme case  $\mathbf{A}_\epsilon^{(1)} :: \mathbf{A}_\epsilon^{(2)} = 0$ ) and then the rate of accumulation is increased ( $f_\pi > 1$ ), Figure 17. The function  $f_\pi$  which enters (5) takes this effect into account.

Let us introduce the 4-th rank back polarization tensor  $\pi$  which represents the polarization in the recent history of cyclic deformation. The rate of accumulation is proposed to be a function of the angle  $\alpha = \arccos(\mathbf{A}_\epsilon :: \pi)$  between the current polarization  $\mathbf{A}_\epsilon$  and  $\pi$ , Figure 20.

The product  $0 \leq \pi :: \mathbf{A}_\epsilon \leq 1$  reflects the degree of adaptation of the soil structure to the current polarization. During cycles with  $\mathbf{A}_\epsilon = \text{const}$  the tensor  $\pi$  is evolving, asymptotically approaching the current polarization,  $\pi \rightarrow \mathbf{A}_\epsilon$ . Since both  $\pi$  and  $\mathbf{A}_\epsilon$  are unit tensors the evolution of  $\pi$  is a kind of *rotation* diminishing the angle  $\alpha$ , Figure 20.

The angle  $\alpha$  is proposed to evolve according to

$$\dot{\alpha} = -C_{\pi 2} \alpha (\epsilon^{\text{ampl}})^2 \quad (24)$$

meaning that the rate of change of  $\alpha$  is proportional to  $-\alpha$  and to the square of the amplitude. The constant  $C_{\pi 2}$  is positive so the back polarization indeed tends towards the current polarization,  $\pi \rightarrow \mathbf{A}_\epsilon$ . In order to update  $\pi$  we rotate it,

$$\pi + \Delta\pi = \mathcal{R} :: \pi, \quad (25)$$

by the angle  $\Delta\alpha = \dot{\alpha}\Delta N$ , wherein the rotation operator is defined by

$$\mathcal{R} = (\cos \Delta\alpha - 1)(\boldsymbol{\mu} \otimes \boldsymbol{\mu} + \boldsymbol{\nu} \otimes \boldsymbol{\nu}) + \sin \Delta\alpha(\boldsymbol{\nu} \otimes \boldsymbol{\mu} - \boldsymbol{\mu} \otimes \boldsymbol{\nu}) + \mathbf{J} \quad (26)$$

and where  $\boldsymbol{\mu} = \mathbf{A}_\epsilon + \pi$  and  $\boldsymbol{\nu} = \mathbf{A}_\epsilon - \pi$  denote mutually orthogonal tensors constructed on the hyperplane perpendicular to the rotation axis.  $\mathbf{J}$  denotes the 8-th rank identity tensor.

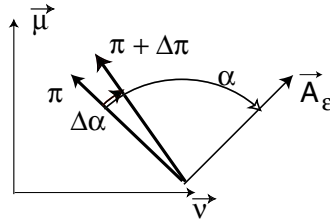


**Fig. 20.** Evolution of  $\pi$  can be seen as a rotation in 6-D space.

An increase in the rate of accumulation can be described by the factor

$$f_\pi = 1 + C_{\pi 1} (1 - \cos \alpha) . \quad (27)$$

The material constants  $C_{\pi 1}$  and  $C_{\pi 2}$  can be determined from an increased accumulation rate due to a rapid change of polarization, Figure 17. The presented tests have been carried out in our multiaxial direct simple shear (DSS) device. Its novelty lies in a possibility of the lower end plate to move (cyclically) along an arbitrary horizontal trajectory, [41].

Let us begin a DSS test applying a large number of  $\epsilon_{13}$ -cycles, Figure 17. At first the back polarization tensor  $\boldsymbol{\pi}$  is undetermined but according to (24) it must tend asymptotically (with  $N$ ) to the stationary value  $\boldsymbol{\pi} = \mathbf{A}_\epsilon$  corresponding to  $f_\pi \approx 1$ . After several hundred cycles  $\boldsymbol{\pi}$  may be expected to have reached this asymptotic value. Then the polarization  $\mathbf{A}_\epsilon$  of the applied loading is rapidly rotated, whereas  $\boldsymbol{\pi}$  is left unchanged. In Figure 17 the  $\epsilon_{13}$ -shearing is followed by the orthogonally polarized  $\epsilon_{23}$ -shearing. This change of polarization corresponds to  $\alpha = 90^\circ$ . According to (27) the rate of accumulation of the axial strain recorded during the test must increase  $f_\pi = (1 + C_{\pi 1})$ -times with respect to the rate of accumulation under the previous  $\epsilon_{13}$ -cycles. Knowing this increase one can determine  $C_{\pi 1}$ . Further, it can be seen from Figure 17 that the additional rate of accumulation declines with  $N$  vanishing completely after several hundred cycles. The solid curve corresponding to  $\epsilon_{23}$ -cycles becomes parallel to the dashed curve of  $\epsilon_{13}$ -cycles. The constant  $C_{\pi 2}$  can be found fitting the measured curve  $f_\pi(N)$  with  $f_\pi(N) = 1 + C_{\pi 1} [1 - \cos(\alpha_0 \exp[-C_{\pi 2}(\epsilon^{\text{amp1}})^2(N - N_0)])]$  for  $N \geq N_0$ , wherein  $N_0$  is the number of cycles prior to the rapid change of polarization. This formula can be easily derived integrating  $\dot{\alpha}$  from (24) with respect to  $N$  and substituting the result (i.e.  $\alpha$ ) into (27).

For in-situ soils subjected to a vertical cyclic preloading  $\boldsymbol{\pi}$  may be initiated with

$$\boldsymbol{\pi} = \mathbf{A}_\epsilon = \mathbf{r} \otimes \mathbf{r} , \quad (28)$$

wherein  $\mathbf{r}$  corresponds to the vertical compression. The spectrum of  $\boldsymbol{\pi}$  is  $\{0, 0, 0, 0, 0, 0, 0, 1\}$  and the non-zero eigenvalue corresponds to the prescribed eigenvector  $\mathbf{r}$ . Another extreme example could be a fresh sand fill with a perfectly *isotropic structure*, i.e. with no privileged direction of cyclic strain. The corresponding back polarization

$$\boldsymbol{\pi}^{\text{iso}} = \frac{1}{3} \mathbf{J} \quad (29)$$

can be obtained integrating the dyadic product  $\mathbf{r} \otimes \mathbf{r}$  over all directions in the strain space and dividing the result by the surface of the 6-dimensional hypersphere.

#### 4 Deformations delayed by the pore water

Let us consider a saturated soil stratum of height  $H$  in an axisymmetric average state subjected to fast cyclic shearing (do to a shear wave caused by an earthquake). Our constitutive relation can be simplified to

$$\begin{Bmatrix} \dot{T}_v \\ \dot{T}_h \end{Bmatrix} = \begin{bmatrix} E_{vv} & E_{vh} \\ E_{hv} & E_{hh} \end{bmatrix} \cdot \begin{Bmatrix} D_v - D_v^{\text{acc}} - D_v^{\text{pl}} \\ D_h - D_h^{\text{acc}} - D_h^{\text{pl}} \end{Bmatrix}, \quad (30)$$

wherein the indices  $_h$  and  $_v$  denote the horizontal and the vertical components, respectively. Large  $H$  and high frequency of cyclic loading may hamper the dissipation of the excess pore water pressures  $u_{\text{gen}}$  generated by pseudo-relaxation of the effective stress  $\mathbf{T}$ . For simplicity we treat the soil as if the were practically undrained. Assuming homogeneity in the horizontal direction we have  $D_h = 0$  and due to the equilibrium condition in the vertical direction the total vertical stress must remain constant, i.e.

$$\dot{T}_v - \dot{u} = 0 \quad (31)$$

We subdivide the whole volume of soil into thin horizontal layers  $I = 1, \dots, M$  of equal heights. The accumulation rate may vary with  $I$  but all layers should have a common  $\dot{u}_{\text{gen}}$  (except for the well drained layers very close to the surface). The generation of the excess pore water pressure  $u$  is (similarly as its dissipation) a non-local phenomenon, i.e.  $\dot{u}_I$  is not a function of  $\mathbf{D}_I^{\text{acc}}$  alone. In saturated soil the excess pressures  $u_{\text{gen}I}$  are almost immediately equalized (much faster than in the consolidation process because of small compressibility of water  $1/K_w \approx 0.5 \cdot 10^{-6} \text{ kPa}^{-1}$ ). To allow for this equalization we cannot assume  $D_{vI} = 0$  for each  $I$ . Instead we impose a *global undrained condition*

$$0 = \sum_{I=1}^M D_{vI} \quad (32)$$

and determine the common  $\dot{u}$  and the individual  $D_{vI}$ -s writing (31) for each layer

$$-\dot{u}_{\text{gen}} \dot{T}_{vI} = -\dot{u}_{\text{gen}} + E_{vvI} (\dot{\epsilon}'_{vI} - D_{vI}^{\text{acc}}) + E_{vhI} (0 - D_{hI}^{\text{acc}}) \quad (33)$$

As a solution (neglecting, at first, the plastic strain rate) we obtain

$$\dot{T}_{vI} = \dot{u}_{\text{gen}} = - \frac{\sum_{I=1}^M D_{vI}^{\text{acc}} + \sum_{I=1}^M D_{hI}^{\text{acc}} E_{hvI} / E_{vvI}}{\sum_{I=1}^M 1 / E_{vvI}} \quad (34)$$

then

$$D_{vI} = \frac{\dot{u}_{\text{gen}}}{E_{vvI}} + D_{vI}^{\text{acc}} + \frac{E_{vhI}}{E_{vvI}} D_{hI}^{\text{acc}} \quad (35)$$

and finally

$$\dot{T}_{hI} = E_{hvI} (\dot{\epsilon}'_{vI} - D_{vI}^{\text{acc}}) + E_{hhI} (0 - D_{hI}^{\text{acc}}) \quad (36)$$

Note that  $\dot{u}_{\text{gen}}$  denotes the *common* rate of the excess pore pressure rate so we have dropped the index  $I$ . The bulk stiffness  $K_w$  of water does not appear in the solution for the strain rate  $\dot{\epsilon}$ . Admittedly, the strain rate  $D_v$  depends also on  $K_w$  i.e. on the deformation of water and soil grains but this is a purely reversible portion of settlement which disappears during the dissipation the excess pore pressure. Therefore it has been neglected.

#### 4.1 Stress and strain rates during reconsolidation

Although the pore pressure build up and dissipation occur simultaneously we consider them as if they acted sequentially, say in each period of cyclic excitation. The dissipation the pore pressure rate (usually negative) is denoted as  $\dot{u}_{\text{diss}}$ . During the (re)consolidation the stress is transferred from water to soil skeleton while satisfying equilibrium condition (31). This process is governed by the well known dissipation equation

$$\frac{\partial u_{\text{diss}}}{\partial t} = c_v \frac{\partial^2 u_{\text{diss}}}{\partial^2 x} \quad \text{wherein } c_v = \frac{kE_{vv}}{\rho_w g}, \quad (37)$$

The reconsolidation results in a pore pressure rate  $\dot{u} = \dot{T}_v$ , the vertical strain rate  $D_v$  and the effective horizontal stress increment  $\dot{T}_h$  (seepage forces are neglected). They can be easily found from the following equation system

$$\begin{Bmatrix} \dot{T}_v = \dot{u}_{\text{diss}} \\ \dot{T}_h \end{Bmatrix} = \begin{bmatrix} E_{vv} & E_{hv} \\ E_{vh} & E_{hh} \end{bmatrix} \cdot \begin{Bmatrix} D_v \\ 0 \end{Bmatrix} \quad (38)$$

Again we have assumed that the reconsolidation is elastic and the problem is homogeneous in horizontal direction,  $D_h = 0$ . As the solution one obtains

$$\dot{T}_h = \frac{E_{hv} \dot{u}_{\text{diss}}}{E_{vv}} \quad \text{and} \quad D_v = \frac{\dot{u}_{\text{diss}}}{E_{vv}} \quad (39)$$

#### 4.2 Corrections for stress and plastic strain

Numerically, after a fast application of a large package of cycles the resulting effective stress may lie outside the elastic range (despite concurrent consolidation). In such case a return mapping of stress onto the yield surface is necessary. Not only the stress correction but also the correction of strain must accompany this mapping. The plastic strain rate  $\mathbf{D}^{\text{pl}} \neq \mathbf{0}$  cannot be neglected.

Assuming  $\mathbf{D}^{\text{pl}} = \mathbf{0}$  we actually computed an elasto-cumulative predictor  $\mathbf{T}^e$  of stress  $\mathbf{T}$ . If our predictor lies outside the yield surface, say Coulomb

pyramid, say  $T_v^e/T_h^e < K_a$  or  $T_v^e/T_h^e > K_p$ , we have to calculate the correction  $\mathbf{c}_T = \dot{\mathbf{T}} - \dot{\mathbf{T}}^e$  of the stress rate and the correction  $\mathbf{c}_D = \mathbf{D} - \mathbf{D}^e$  of the strain rate. Due to the homogeneity in  $x_h$  we have  $c_{\epsilon h} = 0$ . It is convenient to assume correction  $c_{\sigma v} = 0$  because the pore pressure need not be corrected,  $c_u = 0$ . Therefore  $c_{Th} = K_a T_v^e - T_h^e$ .

Let us subtract by sides

$$\dot{\mathbf{T}} = \mathbf{E} : (\mathbf{D} - \mathbf{D}^{\text{acc}} - \mathbf{D}^{\text{pl}}) \quad (40)$$

$$\dot{\mathbf{T}}^e = \mathbf{E} : (\mathbf{D}^e - \mathbf{D}^{\text{acc}}) \quad (41)$$

and express the plastic strain rate by  $\mathbf{D}^{\text{pl}} = \dot{\lambda} \mathbf{m}$ , wherein the flow rule  $\mathbf{m}$  is known. The unknown plastic multiplier  $\dot{\lambda}$  has to be determined. The resulting system of equations

$$\begin{Bmatrix} 0 \\ c_{\sigma h} \end{Bmatrix} = \begin{bmatrix} E_{vv} & E_{vh} \\ E_{hv} & E_{hh} \end{bmatrix} \cdot \begin{Bmatrix} c_{\epsilon v} - \dot{\lambda} m_v \\ 0 - \dot{\lambda} m_h \end{Bmatrix} \quad \text{for soil} \quad (42)$$

can be easily solved and the corrections can be added to  $T_h^e$  and to  $\mathbf{D}^e$ .

If a soil layer is liquefied (the effective stress vanishes,  $Tb = \mathbf{0}$ ) then the accumulation term  $\mathbf{D}^{\text{acc}}$  cannot generate an additional pore pressure  $\dot{u}_{\text{gen}}$  because according to (31) the effective stress would be positive (tension). The pressure dependent stiffness vanishes so the effective stress rate  $\dot{\mathbf{T}} = \mathbf{0}$  is uncoupled from the deformation rate. However, assuming a small residual stiffness and performing computing the necessary corrections mapping the tensile effective stress to the vertex of the Coulomb pyramid a latent accumulation of deformation can be calculated, as discussed in Fig. 6.

## 5 Examples of FE-calculation

The presented model has been implemented into an FE program ABAQUS as a user material subroutine. Remarks on this implementation can be found in [26]. Two boundary value problems will be presented here: settlement of a strip foundation under a pulsating vertical load and differential settlement of a pair of strip foundations on a non-uniform subsoil.

### 5.1 Settlement of a strip foundation

We simulate a centrifuge model test (under increased gravity of  $20g$ ), Figure 21. In this test [9] a strip foundation (with a prototype width  $b = 1$  m) was placed without embedment on a freshly pluviated dense fine sand ( $\rho_s = 2,66$  g/cm<sup>3</sup>,  $e_{\text{min}} = 0.575$ ,  $e_{\text{max}} = 0.908$ ,  $d_{50} = 0.21$  mm,  $U = d_{60}/d_{10} = 1.95$ ,  $I_D \approx 0.90$ ) and cyclically loaded between 4 % and 47 % of the static bearing capacity of 345 kN. The vertical load was chosen as  $Q^{\text{av}} = 88.7$  kN,  $Q^{\text{amp}} = 75.1$  kN and the frequency was 0.44 Hz. Several load-settlement curves

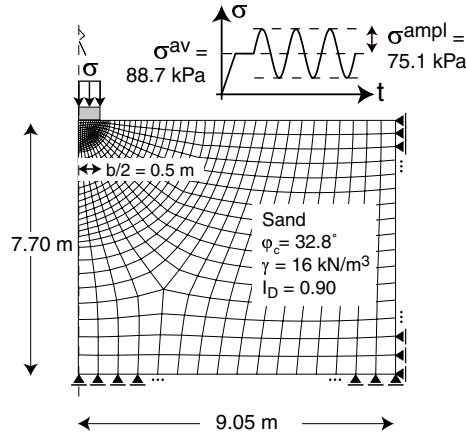


Fig. 21. Geometry of the prototype and soil parameters of the centrifuge test.

generated by the cycles 1-100, as well as the cycle 500, ... are plotted in Figure 22 (prototype scale). The vertical displacement amplitude was  $s^{ampl} = 0.8$  mm and the accumulated settlement after  $N = 10^5$  cycles was  $s = 7.3$  cm.

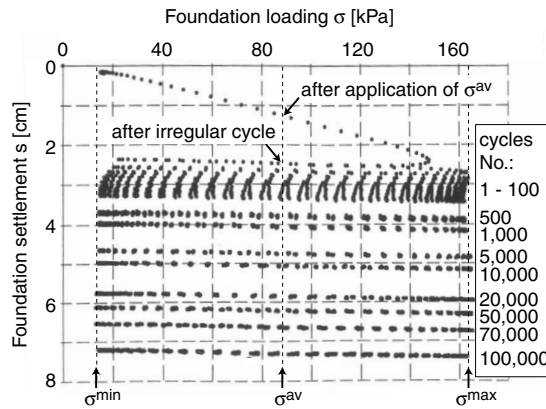
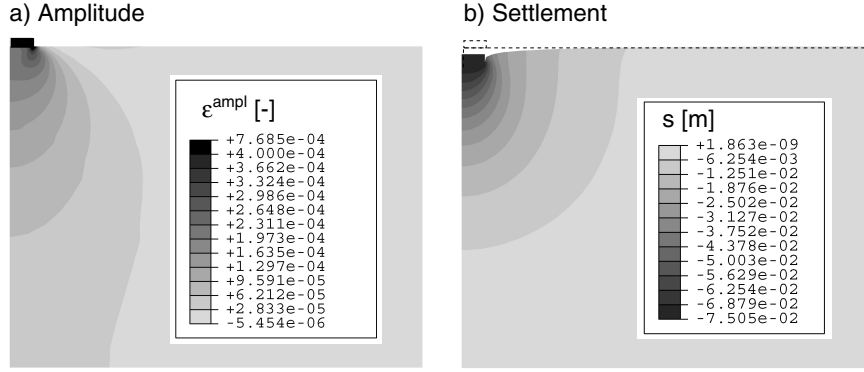


Fig. 22. Settlement of the foundation in the centrifuge test as a function of the number of cycles.

The sand used in the centrifuge test was similar (but not identical) to the laboratory sand described in this paper. Therefore several material constants  $C_{N1} = 1.21 \cdot 10^{-3}$ ,  $C_{N2} = 0.39$ ,  $C_{N3} = 5.7 \cdot 10^{-5}$ ,  $C_e = 0.52$  and  $e_{ref} = 0.908$  have been determined in additional tests. The remaining constants are assumed equal to the ones of the laboratory sand, see Table 2.



**Fig. 23.** a) Field of strain amplitude  $\varepsilon^{\text{ampl}}$ , b) Field of accumulated settlement  $s^{\text{acc}}$  after  $N = 100,000$  cycles

**Table 2.** Material constants of the accumulation model for the 'centrifuge sand'.

$\varepsilon_{\text{ref}}^{\text{ampl}}$	$C_{N1}$	$C_{N2}$	$C_{N3}$	$C_p$	$p_{\text{ref}}$	$C_Y$	$C_e$	$e_{\text{ref}}$
[-]	[-]	[-]	[-]	[-]	[kPa]	[-]	[-]	[-]
$10^{-4}$	$1.21 \cdot 10^{-3}$	0.39	$5.7 \cdot 10^{-5}$	0.43	100	2.0	0.52	0.908

The hypoplasticity constants in Table 3 have been determined from standard laboratory tests except for  $m_T$ ,  $m_R$  and  $\beta_R$  which had been taken from the literature [10, 23, 25] and then slightly adjusted to improve the simulation of the second cycle of the centrifuge test ( estimation of amplitude).

**Table 3.** Material constants of the hypoplastic model used in the implicit steps.

$\varphi_c$	$h_s$	$\nu$	$n$	$e_{d0}$	$e_{c0}$	$e_{i0}$	$\alpha$	$\beta$	$R$	$m_R$	$m_T$	$\chi$	$\beta_R$
[°]	[MPa]	[-]	[-]	[-]	[-]	[-]	[-]	[-]	[-]	[-]	[-]	[-]	[-]
32.8	150	0.2	0.40	0.575	0.908	1.044	0.12	1.0	$10^{-4}$	6.5	3	6	0.1

The FE-calculation was commenced from the geostatic stress with  $K_0 = 0.43$ . The initial cyclic history has been assumed  $g^A = 0$  because the centrifuge test was performed on freshly pluviated sand. Only a half of the  $18.10 \times 7.70$  m subsoil ( prototype dimensions) has been discretized taking advantage of the symmetry. Quadrilateral 8-nodal elements have been used with reduced integration and an hourglass mode control.

Figure 23a presents the resulting field of the strain amplitude  $\varepsilon^{\text{ampl}}$ . The field of the numerically obtained settlements  $s$  after 100,000 cycles is presented in Figure 23b, in particular the settlement of the foundation is  $s = 7.5$  cm. The calculated settlement  $s(N)$  is compared to the measured test values in

Figure 24. The calculated and measured curves are in a fairly good agreement

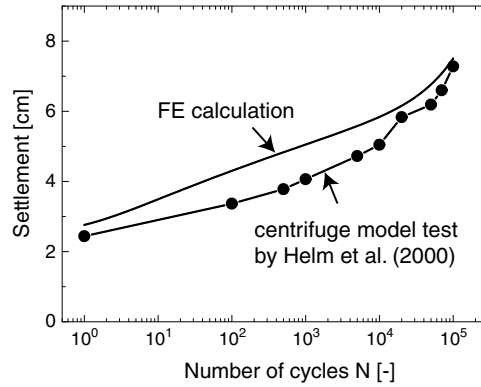


**Fig. 24.** Accumulation of foundation settlement during the regular cycles: FE calculation versus model test.

At the beginning of the simulation some discrepancy between measured and calculated data was caused by an inaccurate prediction of the residual settlement after the irregular cycle. Discussion of this discrepancy is irrelevant in this paper because the implicit model is responsible for it.

The numerical performance of the presented model is satisfactory. The mesh dependence becomes noticeable only for relative coarse discretizations (less than 100 elements). In order to allow for the automatic time incrementation the number of cycles  $N$  has been set to be identical to the 'step-time' in the *pseudo creep* mode. It is recommended to begin calculations in the *pseudo creep* mode from a small increment (we have started with  $\Delta N = 0.01$ ). The time step is promptly increased to  $\Delta N = 500$  cycles or more.

## 5.2 Differential settlement of a pair of strip foundations

Next we investigated an interesting problem of differential settlement of two strip foundations of the width 1m each involving the statistics. The axial distance between the foundations is 6m, Fig. 25. In order to obtain differential settlements a random (spatially correlated) subsoil is generated and subjected to monotonous and cyclic loading (plane strain). Only the void ratio is assumed inhomogeneous. Its spatial variability has been described by the following isotropic autocorrelation function:

$$C_{ij} = \sigma^2 \exp\left(-\frac{\|\mathbf{x}_i - \mathbf{x}_j\|}{\theta}\right) \quad \text{with} \quad \sigma = \frac{1}{2}(e_{\max} - e_{\min}) \quad (43)$$

We assume  $e_{\max} = 1.0$ ,  $e_{\min} = 0.6$ , the average void ratio is  $\bar{e} = 0.8$ . Three correlation lengths have been tried out  $\theta = 0.5\text{m}$ ,  $2.0\text{m}$  and  $20\text{m}$ . We are using

1098 elements with 4 Gauss points per element, which results in a  $(4392 \times 4392)$  covariance matrix. In order to obtain an autocorrelated void ratio field the matrix  $\mathbf{C}$  is subjected to spectral decomposition

$$\mathbf{C} = \mathbf{\Phi} \cdot \mathbf{\Lambda} \cdot \mathbf{\Phi}^T. \quad (44)$$

with  $n$  eigenvalues collected in  $\mathbf{\Lambda} = \text{diag}\{\lambda_1, \dots, \lambda_n\}$  and with an orthogonal matrix  $\mathbf{\Phi}$  composed of eigenvectors (in columns). Finally, the field  $e(\mathbf{x})$  is generated with

$$e'(\mathbf{x}) = \bar{e} + \sum_{i=1}^n r_i^{[-1,1]} \frac{1}{2} \sqrt{\lambda_i} \mathbf{\Phi}_i \quad (45)$$

wherein  $r^{[-1,1]} = 2r^{[0,1]} - 1$  is a uniform variate (random real number with constant probability density function) from the range  $[-1, 1]$ .

The void ratio fields have been generated using the user initial stress and the user initial state routines of ABAQUS. More than 30 stochastic fields  $e(\mathbf{x})$

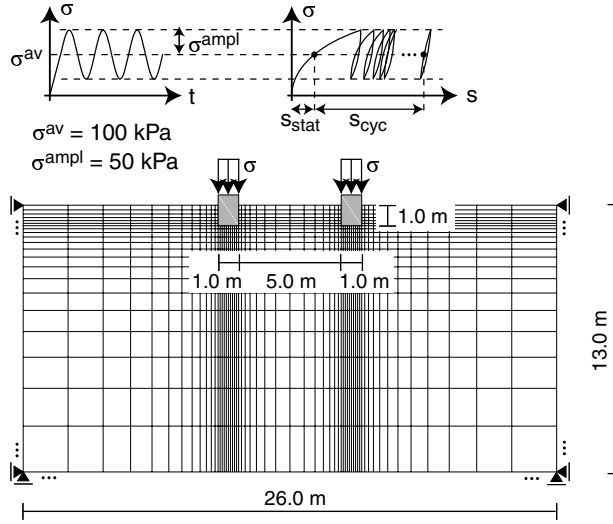


**Fig. 25.** BVP and FE mesh for two strip foundations

with corresponding stress fields  $\mathbf{T}(xb)$  have been generated using (45). Examples of void ratio fields are presented in Fig. 26. Although equally loaded (at first monotonically and then cyclically) the foundations exhibit a differential settlement  $\Delta s$  which for each calculation is normalized by the mean settlement  $\bar{s}$ .

The calculation reveals that the autocorrelated fields  $e(\mathbf{x})$  imply an almost linear relation between  $\Delta s/\bar{s}$  calculated after monotonic loading on one hand and  $\Delta s/\bar{s}$  obtained in the process of cyclic accumulation (after  $10^5$  cycles) on the other hand, Fig. 27.

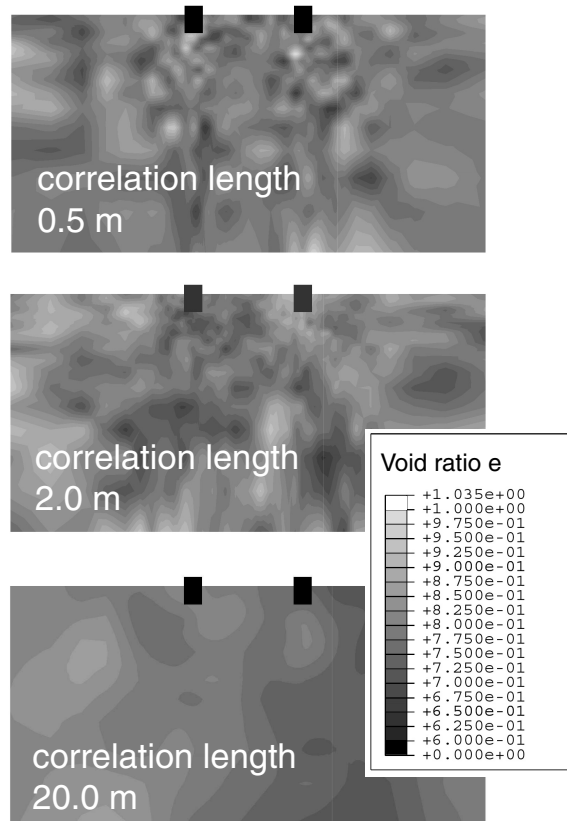


**Fig. 26.** Void ratio distributions generated using different correlation lengths  $\theta$ .

It can be seen from Fig. 27 that the settlement  $\bar{s}$  due to cyclic loading is accompanied by a three times larger differential settlement  $\Delta s$  than in the static case. An explanation of this effect is the fact that the cyclic accumulation is proportional to the square of the strain amplitude, see Eq. ??, whereas the static settlement is approximately proportional to the load i.e. to the amplitude. Therefore cyclic accumulation is a short-range phenomenon (involves the soil volume only in the vicinity of the foundation). The probability of finding an extreme dense zone of sand under one foundation and an extreme loose zone under the other one is therefore higher in the case of cyclic loading.

## 6 ACKNOWLEDGEMENTS

The authors are grateful to DFG (German Research Council) for the financial support. This study is a part of the subproject A8 "Influence of the fabric

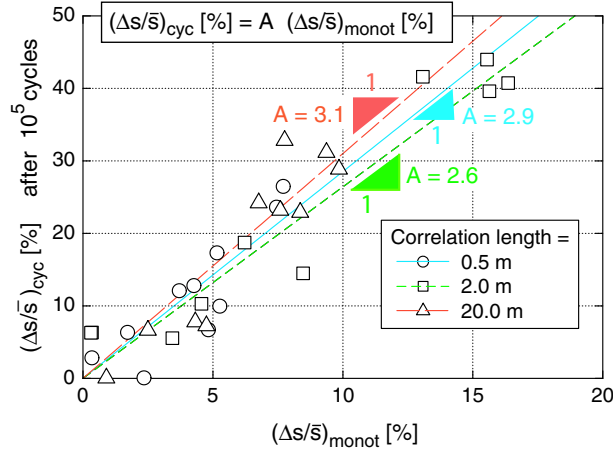


**Fig. 27.** Indirect limitation of differential settlement via total settlement should be three times more restrictive in case of cyclic loads. This result seems to be independent of the correlation length  $\theta$  within the tested range.

change in soil on the lifetime of structures” of SFB 398 ”Lifetime oriented design concepts”.

## 7 APPENDIX A

Vectors and tensors are distinguished by bold typeface, for example  $\mathbf{T}$ ,  $\mathbf{v}$  or in sans serif font (e.g.  $\mathbf{E}$ ). The symbol  $\cdot$  denotes multiplication with one dummy index (single contraction), e.g. the scalar product of two vectors can be written as  $\mathbf{a} \cdot \mathbf{b} = a_k b_k$ . Multiplication with two dummy indices (double contraction) is denoted with a colon, e.g.  $\mathbf{A} : \mathbf{B} = \text{tr}(\mathbf{A} \cdot \mathbf{B}^T) = A_{ij} B_{ij}$ , wherein  $\text{tr} \mathbf{X} = X_{kk}$  reads trace of a tensor. The superscript  $\square^T$  denotes transposition. Analogously we may define double colon  $::$  to quadruple contraction with four dummy indices. Two fourth order identity tensors with symmetrization  $I_{ijkl} = \frac{1}{2}(\delta_{ik}\delta_{jl} + \delta_{il}\delta_{jk})$  and without symmetrization  $J_{ijkl} = \delta_{ik}\delta_{jl}$  are used. The brackets  $\| \cdot \|$  denote the Euclidean norm. The deviatoric part of a tensor is denoted by an asterisk, e.g.  $\mathbf{T}^* = \mathbf{T} - \frac{1}{3} \mathbf{1} \text{tr} \mathbf{T}$ , wherein  $(\mathbf{1})_{ij} = \delta_{ij}$  stands for the Kronecker’s symbol. The operator  $(\cdot)_{ij}$  extracts the  $ij$ -th component from the tensor in brackets. Permutation symbol is denoted by  $e_{ijk}$ . Dyadic multiplication is written with  $\otimes$ , e.g.  $(\mathbf{a} \otimes \mathbf{b})_{ij} = a_i b_j$  or  $(\mathbf{T} \otimes \mathbf{1})_{ijkl} = T_{ij} \delta_{kl}$ . Positively proportional quantities are denoted by a tilde, e.g.  $\mathbf{T} \sim \mathbf{D}$ . Normalized quantities are denoted by an arrow and tensors divided by their traces are denoted with a hat, for example  $\hat{\mathbf{D}} = \mathbf{D} / \|\mathbf{D}\|$  and  $\hat{\mathbf{T}} = \mathbf{T} / \text{tr} \mathbf{T}$ . The sign convention of general mechanics with *tension positive* is obeyed. The superposed dot,  $\dot{\square}$ , denotes the material rate (with respect to  $N$ ) and the superposed

circle  $\dot{\square}$  denotes the Zaremba-Jaumann rate ( finite rotations are accounted for).

The effective Cauchy stress  $\mathbf{T}$ , the stretching  $\mathbf{D}$  and the total deformation is expressed by the logarithmic strain  $\boldsymbol{\epsilon} = \ln \mathbf{U}$  is used throughout the text ( $\mathbf{U}$  denotes the right stretch tensor). Generally, it would be inaccurate to interpret  $\mathbf{D}$  as a time derivative of the strain  $\boldsymbol{\epsilon}$  given by (52). In the axisymmetric case, alternatively to the popular Roscoe's variables:

$$p = -(T_1 + T_2 + T_3)/3; q = -T_1 + (T_2 + T_3)/2 \quad (46)$$

$$\epsilon_v = -(\epsilon_1 + \epsilon_2 + \epsilon_3); \quad \epsilon_q = -\frac{2}{3}(\epsilon_1 - \frac{1}{2}(\epsilon_2 + \epsilon_3)) \quad (47)$$

$$D_v = -(D_1 + D_2 + D_3); D_q = -(2D_1 - D_2 - D_3)/3, \quad (48)$$

the 'normalized', or isomorphic variables [23] :

$$P = \sqrt{3}p, \quad Q = \sqrt{\frac{2}{3}}q, \quad (49)$$

$$\epsilon_P = \frac{1}{\sqrt{3}}\epsilon_v, \quad \epsilon_Q = \sqrt{\frac{3}{2}}\epsilon_q \quad (50)$$

$$D_P = \frac{1}{\sqrt{3}}D_v, \quad D_Q = \sqrt{\frac{3}{2}}D_q \quad (51)$$

are used. The isomorphic variables preserve orthogonality and distance. Note that  $P^2 = \|\frac{1}{3} \mathbf{1tr} \mathbf{T}\|^2$ ;  $Q^2 = \|\mathbf{T}^*\|^2$  and  $D_P^2 = \|\frac{1}{3} \mathbf{1tr} \mathbf{D}\|^2$ ;  $D_Q^2 = \|\mathbf{D}^*\|^2$  hold. In the 6-D space the isomorphic components of strain are

$\{\epsilon_{11}, \epsilon_{22}, \epsilon_{33}, \sqrt{2}\epsilon_{12}, \sqrt{2}\epsilon_{13}, \sqrt{2}\epsilon_{23}\}$  and  
 $\{T_{11}, T_{22}, T_{33}, \sqrt{2}T_{12}, \sqrt{2}T_{13}, \sqrt{2}T_{23}\}$ .

The Matsuoka-Nakai [19] inequality  $-I_1 I_2 / I_3 - (9 - \sin^2 \varphi_c) / (1 - \sin^2 \varphi_c) \leq 0$  with the critical friction angle  $\varphi_c$  is used throughout this paper as the yield criterion. It is formulated using the basic invariants of the stress tensor:  $I_1 = \text{tr} \mathbf{T}$ ,  $I_2 = [\mathbf{T} : \mathbf{T} - (\text{tr} \mathbf{T})^2] / 2$  and  $I_3 = \det \mathbf{T}$ .

Quantifying the OOP-cycles (Section 3) one should account for the rotation of the principal strain axes within a cycle but disregard the rigid body rotation. This is done if the strain  $\boldsymbol{\epsilon}$  is calculated with respect to the material frame of reference. In the presented model the logarithmic strain is defined with respect to the initial material configuration (usually  $K_0$ -state) as

$$\boldsymbol{\epsilon} = \ln \mathbf{U} = \mathbf{R}^T \cdot \ln \mathbf{V} \cdot \mathbf{R}, \quad (52)$$

wherein  $\mathbf{V}$  and  $\mathbf{U}$  denote the left and the right stretch tensor and  $\mathbf{R}$  is the rotation tensor appearing in the polar decomposition of the deformation gradient. We had to 'unrotate' the total strain because it is defined as  $\ln \mathbf{V}$  in the FE program ABAQUS.

## 8 APPENDIX B

Working with a typical settlement formula

$$s(N) = s_1 f(N) \quad (53)$$

one assumes that the information about the cyclic history can be obtained from the residual settlement after a single cycle, usually from  $s_1$  after the first one. The derivative of  $s(N)$  with respect to  $N$  describes the settlement per cycle, e.g. the settlement due to the  $K$ -th cycle is

$$s_K = \left. \frac{ds(N)}{dN} \right|_{N=K} = s_1 f'(K) \quad (54)$$

Of course, in order to be objective, the predicted settlement due to a given cycle should not depend on how we count cycles (i.e., which cycle we call "the first"). Therefore, beside fitting the experimental observation, the function  $f(N)$  must satisfy the objectivity criterion:

$$s'(N) = s_1 f'(N) = s_M f'(N - M) \quad (55)$$

in which  $s_M$  is the settlement due to an arbitrarily chosen cycle No.  $M$  (because someone may consider  $M$  as the 'first' cycle). Substituting  $s_M$  from (54) into (55) the objectivity condition takes the form

$$f'(N) \equiv f'(M) f'(N - M) \quad (56)$$

it can be shown that the widely used functions  $f(N) = N^C$  or  $f(N) = 1 + C \log(N)$ , cf. [11,28], do not satisfy this condition. An objective (consistent) settlement formula is

$$s(N) = s_1 \frac{1}{C} [1 - \exp(-CN)] \quad (57)$$

wherein  $C$  is a positive material constant. Indeed, one can conclude from (56) that  $f'(N)$  has the form

$$f'(N) = \exp(-CN). \quad (58)$$

After integration of  $f'(N)$  with respect to  $N$  with the initial condition  $f(0) = 0$  we arrive at (57).

## References

1. R. D. Barksdale. Laboratory evaluation of rutting in base course materials. In *Third International Conference on Structural Design of Asphalt Pavements*, volume 3, pages 161–174, 1972.

2. G. Bouckovalas, R. V. Whitman, and W. A. Marr. Permanent displacement of sand with cyclic loading. *Journal of Geotechnical Engineering*, 110(11):1606–1623, 1984.
3. J. L. Chaboche. Constitutive equations for cyclic plasticity and cyclic viscoplasticity. *International Journal of Plasticity*, 5:247–302, 1989.
4. J. L. Chaboche. Modelling of ratchetting: evaluation of various approaches. *European Journal of Mechanics*, 13(4):501–518, 1994.
5. C. Chopi and P. Arduino. Behavioral characteristics of gravelly soils under general cyclic loading conditions. In T. Triantafyllidis, editor, *Cyclic Behaviour of Soils and Liquefaction Phenomena*, pages 115–122. Balkema, March/April 2004. International Conference in Bochum, 31 March - 02 April 2004.
6. M. R. Coop. On the mechanics of reconstituted and natural sands. In H. Di Benedetto, T. Doanh, H. Geoffroy, and Sauzéat C., editors, *Deformation characteristics of geomaterials. Recent investigations and prospects.*, pages 29–58. Balkema, 2005.
7. A. Ekberg. *Rolling contact fatigue of railway wheels*. PhD thesis, Chalmers University of Technology, 2000. Solid Mechanics.
8. A. Gotschol. *Veränderlich elastisches und plastisches Verhalten nichtbindiger Böden und Schotter unter zyklisch-dynamischer Beanspruchung*. PhD thesis, Universität Gh Kassel, April 2002.
9. J. Helm, J. Laue, and Th. Triantafyllidis. Untersuchungen an der RUB zur Verformungsentwicklung von Böden unter zyklischen Beanspruchungen. In Th. Triantafyllidis, editor, *Böden unter fast zyklischer Belastung: Erfahrungen und Forschungsergebnisse*, pages 109–133. Lehrstuhl für Grundbau und Bodenmechanik, Ruhr-Universität Bochum, 2000.
10. I. Herle. *Hypoplastizität und Granulometrie einfacher Korngerüste*. PhD thesis, Institut für Boden- und Felsmechanik der Universität Karlsruhe, 1997. Nr. 142.
11. A. Hettler. *Verschiebungen starrer und elastischer Gründungskörper in Sand bei monotoner und zyklischer Belastung*. PhD thesis, Institut für Boden- und Felsmechanik der Universität Karlsruhe, 1981. Heft Nr. 90.
12. P. Hornych, J. F. Corte, and J. L. Paute. Étude des déformations permanentes sous chargements répétés de trois graves non traitées. *Bulletin de Liaison des Laboratoires des Ponts et Chaussées*, 184:77–84, 1993.
13. K. Ishihara. Liquefaction and flow failure during earthquakes. *Géotechnique*, 43(3):351–415, 1993.
14. S. Khedr. Deformation characteristics of granular base course in flexible pavements. In *Transportation Research Record*, volume 1043, pages 131–138, 1985.

15. H.Y. Ko and R.F. Scott. Deformation of sand in hydrostatic compression. *Journal of Soil Mechanics and Foundations Division ASCE*, 93(SM3):137–156, 1967.
16. R. W. Lentz and G. Y. Baladi. Constitutive equation for permanent strain of sand subjected to cyclic loading. In *Transportation Research Record*, volume 810, pages 50–54, 1981.
17. W. A. Marr and J. T. Christian. Permanent displacements due to cyclic wave loading. *Journal of the Geotechnical Engineering Division ASCE*, 107(GT8):1129–1149, 1981.
18. G. R. Martin, W. D. L. Finn, and H. B. Seed. Fundamentals of liquefaction under cyclic loading. *Journal of the Geotechnical Engineering Division ASCE*, 101(GT5):423–439, 1975.
19. H. Matsuoka and T. Nakai. A new failure for soils in three-dimensional stresses. In *Deformation and Failure of Granular Materials*, pages 253–263, 1982. Proc. IUTAM Symp. in Delft.
20. M.A. Miner. Cumulative damage in fatigue. *Transactions of the American Society of Mechanical Engineering*, 67:A159–A164, 1945.
21. Z. Mróz, V. A. Norris, and O. C. Zienkiewicz. An anisotropic hardening model for soils and its application to cyclic loading. *International Journal for Numerical and Analytical Methods in Geomechanics*, 2:203–221, 1978.
22. P. G. Nicholson, R. B. Seed, and H. A. Anwar. Elimination of membrane compliance in undrained triaxial testing. 1. measurement and evaluation. *Canadian Geotechnical Journal*, 30:727–738, 1993.
23. A. Niemunis. *Extended hypoplastic models for soils*. Ruhr-University Bochum, Institute of Soil Mechanics and Foundation Engineering, 2003. 34, available from [www.pg.gda.pl/~aniem/an-liter.html](http://www.pg.gda.pl/~aniem/an-liter.html).
24. A. Niemunis and M. Cudny. On hyperplasticity for clays. *Computers and Geotechnics*, 23:221–236, 1998.
25. A. Niemunis and I. Herle. Hypoplastic model for cohesionless soils with elastic strain range. *Mechanics of Cohesive-Frictional Materials*, 2:279–299, 1997.
26. A. Niemunis, T. Wichtmann, and T. Triantafyllidis. A high-cycle accumulation model for sand. *Computers and Geotechnics*, 32(4):223–315, 2005.
27. A. Niemunis, T. Wichtmann, and Th. Triantafyllidis. Compaction of freshly pluviated granulates under uniaxial and multiaxial cyclic loading. In J. Vanicek et al., editor, *Geotechnical problems with man-made and man-influenced grounds*, volume 1, pages 855–860, August 2003. XIIIth European Conference On Soil Mechanics and Geotechnical Engineering, Prague.

28. N. J. O’Riordan. Effects of cyclic loading on the long term settlements of structures. In M.P. O’Reilly and S.F. Brown, editors, *Cyclic Loading of Soils*, pages 411–433. Blackie Glasgow, 1992.
29. I. V. Papadopoulos. A new criterion of fatigue strength for out-of-phase bending and torsion of hard metals. *International Journal of Fatigue*, 16:377–384, 1994.
30. J. L. Paute, P. Jouve, and E. Ragneau. Modèle de calcul pour le dimensionnement des chaussées souples. *Bulletin de Liaison des Laboratoires des Ponts et Chaussées*, 156:21–36, 1988.
31. K. H. Roscoe and J. B. Burland. On the generalized stress-strain behaviour of wet clays. In J. Heyman and F. A. Leckie, editors, *Engineering plasticity*, pages 535–609. Cambridge University Press, 1968.
32. A. Sawicki. An engineering model for compaction of sand under cyclic loading. *Engineering Transactions*, 35:677–693, 1987.
33. Y. Shamoto, M. Sato, and J-M. Zhang. Simplified estimation of earthquake-induced settlements in saturated sand deposits. *Soils and Foundations*, 36(1):39–50, 1996.
34. A. S. J. Suiker. Fatigue behaviour of granular materials. Technical Report 7-98-119-3, Delft University of Technology, Faculty of Civil Engineering, 1998.
35. A. S. J. Suiker. Static and cyclic loading experiments on non-cohesive granular materials. Technical Report 1-99-DUT-1, Delft University of Technology, Faculty of Civil Engineering, 1999.
36. A. S. J. Suiker and R. de Borst. A numerical model for cyclic deterioration of railway tracks. *International Journal for Numerical Methods in Engineering*, 57:441–470, 2003.
37. G. T. H. Sweere. *Unbound granular bases for roads*. PhD thesis, Delft University of Technology, Netherlands, 1990.
38. T. Triantafyllidis, T. Wichtmann, and A. Niemunis. On the determination of cyclic strain history. In T. Triantafyllidis, editor, *Cyclic Behaviour of Soils and Liquefaction Phenomena*, pages 321–334. Balkema, March/April 2004. International Conference in Bochum, 31 March - 02 April 2004.
39. K. C. Valanis and C. F. Lee. Endochronic theory of cyclic plasticity with applications. *Journal of Applied Mechanics*, 51:367–374, 1984.
40. B. Vuong. Evaluation of back-calculation and performance models using a full scale granular pavement tested with the accelerated loading facility (alf). In *Proceedings 4 th International Conference on the Bearing Capacity of Roads and Airfields, Minneapolis*, pages 183–197, 1994.
41. T. Wichtmann, A. Niemunis, and T. Triantafyllidis. The effect of volumetric and out-of-phase cyclic loading on strain accumulation. In T. Triantafyllidis,

- editor, *Cyclic Behaviour of Soils and Liquefaction Phenomena*, pages 247–256. Balkema, March/April 2004. International Conference in Bochum, 31 March - 02 April 2004.
42. T. Wichtmann, A. Niemunis, and T. Triantafyllidis. Strain accumulation in sand due to drained uniaxial cyclic loading. In T. Triantafyllidis, editor, *Cyclic Behaviour of Soils and Liquefaction Phenomena*, pages 233–246. Balkema, March/April 2004. International Conference in Bochum, 31 March - 02 April 2004.
43. T. Wichtmann, A. Niemunis, and T. Triantafyllidis. Strain accumulation in sand due to cyclic loading: drained triaxial tests. *Soil Dynamics and Earthquake Engineering*, 2005. accepted for publication.
44. H. Wolff and A. T. Visser. Incorporating elasto-plasticity in granular layer pavement design. In *Proceedings of Institution of Civil Engineers Transport*, volume 105, pages 259–272, 1994.

---

## Index

- objective (consistent) settlement, 34
- stress obliquity, 14
- stress tensor, 33
  
- Abaqus, 30
- accumulated pore pressure, 7
- accumulation, 2
- adaptation, 22
- algorithm, 21
- alternating plasticity, 7
- amplitude, 1, 9
- amplitudes in the past, 14
- angularity, 17
- APPENDIX, 32, 34
- area in the strain space, 18
- arrow, 32
- asperity, 17
- associated flow rule, 9
- asymmetry of the strain, 7
- autocorrelated field, 30
- autocorrelated void ratio, 30
- automatic time incrementation, 29
- average, 1
- average mean pressure, 7
- average stress, 8
- average stress ratio, 9
  
- axisymmetric average state, 24
  
- Back polarization, 22
- back polarization, 1, 22
- barotropic, 6
- bearing capacity, 26
- blocks of cycles, 13
- bulk stiffness  $K_w$  of water, 25
  
- Cam-clay model, 9
- Cauchy stress, 33
- centrifuge model, 26
- centrifuge test, 27, 28
- circulation, 20
- clockwise, 20
- coaxial, 19
- coaxiality, 9
- compaction curves, 11
- compliance, 6
- compressibility of water, 24
- compromise solution, 14
- concurrent effects, 12
- conditioning phase, 5
- contraction, 32
- contradiction, 5
- convex loops, 13
- cooling, 5

- correction of strain, 25
- Corrections, 25
- corrections, 26
- correlate, 12
- correlation length, 29, 31, 32
- correlations, 17
- counterclockwise, 20
- covariance matrix, 30
- critical friction angle, 33
- critical state, 16
- critical state line, 9
- CSL, 16
- cumulative errors, 4
- cycle, 1
- cyclic excitation, 25
- Cyclic history, 11
- cyclic preloading, 1, 11
  
- decomposition of the irreversible strain, 5
- deformation gradient, 33
- degeneration, 21
- dense sand, 16
- densification rate, 11
- dependence on the void ratio, 16
- deviatoric component, 9
- deviatoric part, 32
- Differential settlement, 29
- differential settlement, 29–31
- dilative, 9
- direct extrapolation, 7
- discrepancy, 29
- discretized, 28
- dissipation, 24, 25
- dissipation equation, 25
- distance to the critical state, 16
- double contraction, 32
- dummy index, 32
  
- Dyadic multiplication, 32
- dyadic product, 23
  
- earthquake, 24
- effective stress, 24, 25
- eigensensors, 21
- eigenvalues, 21
- elasto-cumulative predictor, 6
- embedment, 26
- endochronic, 4
- equalization, 24
- estimation of amplitude, 28
- Euclidean norm, 32
- Examples of FE, 26
- excess pore water, 24
- explicit calculation, 4
- explicit formula, 4, 7
- extended direct simple shear, 18
- extended hypoplasticity, 4
  
- factor  $f_e$ , 14
- factor  $f_N$ , 11
- factors, 17
- factors  $f_p$  and  $f_e$ , 16
- factors  $f_p$  and  $f_Y$ , 14
- failure, 13
- fatigue analysis, 18
- fatigue loading, 5
- finite rotations, 33
- flattening, 20
- flow rule, 5, 9, 26
- fluctuation of stress, 12
- foundation, 31
- frame of reference, 33
- frequency, 26
- fresh pluviated, 5
- freshly pluviated, 12, 26, 28
- function  $f_\pi$ , 22

- generation of the excess pore water, 24
- global undrained condition, 24
- grain size distribution, 17
- gravity, 26
  
- harmonic functions, 19
- hat, 32
- high cycle models, 1
- high-cycle model, 4
- high-cycle models, 6
- hodograph, 1
- homogeneity, 24
- horizontal trajectory, 23
- hourglass mode, 28
- hyperelasticity, 6
- hyperplane, 20, 22
- hypersphere, 23
- hypoplastic model, 28
- hypoplasticity, 4
  
- identity tensor, 32
- implementation, 26
- implicit calculation, 3
- implicit models, 6
- implicit steps, 28
- in-phase, 17
- in-phase cycles, 2
- in-situ soils, 23
- inaccuracies, 4
- inaccurate, 7
- index of density, 10
- Influence factor  $f_{\text{ampl}}$ , 9
- inhomogeneous spatial distribution, 6
- initial condition, 34
- initial stress, 4
- input parameters, 17
- invariants, 33
- IP, 2, 17
- IP-cycle, 9
- IP-cycles, 18
- irregular cycle, 6, 8, 29
- isomorphic components, 10, 33
- isomorphic variables, 33
- isotropic autocorrelation, 29
- isotropic pseudo-relaxation, 7
- isotropic structure, 23
  
- Kronecker's symbol, 32
  
- laboratory sand, 27
- large amplitudes, 7
- large number of cycles, 12
- largest span, 21
- latent accumulation, 26
- latent densification, 8
- liquefaction potential, 12
- liquefied , 26
- liquefied stage, 8
- logarithmic strain, 33
- loose sand, 16
  
- M-N, 6
- material constant, 34
- Material constants, 28
- material constants, 17, 27
- material rate, 32
- Matsuoka and Nakai, 5, 15
- Matsuoka-Nakai, 33
- mean stress  $p^{\text{av}}$ , 14
- measured response, 3
- membrane penetration, 10
- memorizing the number of cycles, 14
- metals, 18
- Miner's rule, 12
- mixed-control, 2
- Monotonic loading, 8
- multi-surface, 4

- multiaxial, 18
- multiaxial direct simple shear, 23
- multiplication, 32
- multiplicative form, 7
  
- non-local phenomenon, 24
- non-physical state variable, 12
- non-uniform subsoil, 26
- normalized amplitude, 21
- Normalized quantities, 32
- notation, 3
  
- objectivity criterion, 34
- OOP, 2, 17
- OOP-cycle, 9
- orientation, 18, 19, 21
- orthogonal, 21
- oscillation, 19
- out-of-phase, 17
- Out-of-phase cycles, 17
- out-of-phase cycles, 2
- ovality, 18
  
- package of cycles, 22
- packages, 13
- Palmgren-Miner's rule, 13
- parameters, 27
- periodic function, 18
- Permutation, 32
- phase shift, 18, 19
- phenomenological, 12
- plastic deformation, 6
- plastic multiplier, 26
- plastic strain, 5
- plastic strain rate, 25
- plasticity theory, 9
- plastification, 6
- pluviate, 28
- polar decomposition, 33
  
- polarization, 9, 17–19, 21, 22
- polarization tensor, 23
- pore pressure rate, 25
- pore water, 24
- predictor, 6
- pressure-dependent, 16
- principal strain axes, 33
- privileged direction, 23
- probability, 31
- probability density, 30
- progressive failure, 7
- prototype, 26–28
- pseudo-creep, 2
- pseudo-relaxation, 2, 24
- pulsating vertical load, 26
- purified curve, 12
- purified diagrams, 15
  
- Quadrilateral 8-nodal elements, 28
- quadruple contraction, 32
  
- rainflow algorithm, 13
- rate, 5, 32
- rate of accumulation, 2
- Rayleigh waves, 18
- recent history, 22
- recent polarization, 11
- reconsolidation, 25
- recorded cycle, 20
- recording, 4
- reduced integration, 28
- regular cycle, 8
- regular cycles, 29
- residual settlement, 29, 34
- return mapping, 6, 25
- rigid body rotation, 33
- Roscoe's invariants, 9
- Roscoe's variables, 33

- rotation, 22, 33
- rotation axis, 22
- rotation operator, 22
  
- saturated, 24
- saturated soil, 24
- scalar amplitude, 21
- scalar product, 32
- seepage forces, 25
- semi-empirical equation, 7
- sense of the direction, 19
- Sensitivity, 17
- sequence of application, 13
- Settlement, 27
- settlement, 28, 29, 31
- settlement formula, 34
- settlement formulas, 2
- Shamoto, 8
- shape of the strain cycle, 19
- shear bands, 12
- shear wave, 24
- short-range phenomenon, 31
- sign convention, 32
- small-strain nonlinearity, 4
- span, 20, 21
- spans, 19
- spatial variability, 29
- spectral decomposition, 30
- state variable  $g^A$ , 12
- statistics, 29
- stiffening, 5
- stochastic fields, 30
- strain, 33
- Strain amplitude, 6
- strain amplitude, 4
- strain trajectory, 20
- strategies, 3
- stress, 33
- stress amplitude, 6
- stress correction, 25
- stress cycles, 2
- stress invariants, 15
- stretch tensor, 33
- stretching, 33
- strip foundation, 26, 29
- subroutine, 26
- Summary, 17
- symmetrization, 32
  
- tension cut-off, 5
- tensor, 32
- tensorial amplitude, 21
- Tensorial amplitude  $A_\epsilon$ , 19
- tensorial definition, 18
- tensorial strain amplitude, 1
- thermic shrinkage, 5
- tilde, 32
- time step, 29
- total deformation, 33
- total vertical stress, 24
- transposition, 32
- triaxial extension, 9
- typeface, 32
- typical range, 17
  
- undrained, 24
- uniaxial, 18
- uniform variate, 30
- Unsymmetric strain-controlled cycle, 8
- Unsymmetric stress-controlled cycle, 8
- user initial state, 30
- user initial stress, 30
- user material, 26
  
- validity, 9
- vanishing effective stress, 8
- variability, 17

Vector, 32

void ratio, 9, 14

void ratio  $e$ , 14

water pressure, 24

Wöhler's curve, 13

yield criterion, 33

yield surface, 14

Young modulus, 6

Zaremba-Jaumann rate, 3, 33

